Global water cycle shifts far beyond pre-industrial conditions – planetary boundary for freshwater change transgressed

Miina Porkka, Vili Virkki, Lan Wang-Erlandsson, Dieter Gerten, Tom Gleeson, Chinchu Mohan, Ingo Fetzer, Fernando Jaramillo, Arie Staal, Sofie te Wierik, Arne Tobian, Ruud van der Ent, Petra Döll, Martina Flörke, Simon Gosling, Naota Hanasaki, Yusuke Satoh, Hannes Müller Schmied, Niko Wanders, Johan Rockstrom, & Matti Kummu

2022

Faculty of Science

Faculty of Engineering and Computer Science

Faculty Publications

Original citation:

Porkka, M., Virkki, V., Wang-Erlandsson, L., Gerten, D., Gleeson, T., Mohan, C., Fetzer, I., Jaramillo, F., Staal, A., Wierik, S. T., Tobian, A., Van Der Ent, R., Döll, P., Flörke, M., Gosling, S., Hanasaki, N., Satoh, Y., Schmied, H. M., Wanders, N., . . . Kummu, M. (2022). Global water cycle shifts far beyond pre-industrial conditions – planetary boundary for freshwater change transgressed. *EarthArXiv*. https://doi.org/10.31223/x5bp8f

Global water cycle shifts far beyond pre-industrial conditions – planetary boundary for freshwater change transgressed

Miina Porkka[1,2]*†, Vili Virkki[1]*†, Lan Wang-Erlandsson[3,4,5], Dieter Gerten[5,6], Tom Gleeson[7,8], Chinchu Mohan[7,9], Ingo Fetzer[3,4], Fernando Jaramillo[4,10], Arie Staal[11], Sofie te Wierik[12], Arne Tobian[3,5], Ruud van der Ent[13], Petra Döll[14,15], Martina Flörke[16], Simon N. Gosling[17], Naota Hanasaki[18], Yusuke Satoh[19,20], Hannes Müller Schmied[14,15], Niko Wanders[21], Johan Rockström[3,5], Matti Kummu[1]

[1] Water and Development Research Group, Aalto University; Espoo, Finland.
[2] Global Economic Dynamics and the Biosphere, Royal Swedish Academy of Sciences; Stockholm, Sweden.
[3] Stockholm Resilience Centre, Stockholm University; Stockholm, Sweden.
[4] Bolin Centre for Climate Research, Stockholm University; Stockholm, Sweden.
[5] Potsdam Institute for Climate Impact Research (PIK), Member of the Leibniz Association; Potsdam, Germany.
[6] Geography Department and IRI THESys, Humboldt-Universität zu Berlin; Berlin, Germany.
[7] Department of Civil Engineering, University of Victoria; Victoria, British Columbia, Canada.
[8] School of Earth and Ocean Sciences, University of Victoria; Victoria, British Columbia, Canada.
[9] Global Institute for Water Security, University of Saskatchewan; Saskatoon, Saskatchewan, Canada.
[10] Department of Physical Geography, Stockholm University; Stockholm, Sweden.
[11] Copernicus Institute of Sustainable Development, Utrecht University; Utrecht, Netherlands.
[12] Institute for Biodiversity and Ecosystem Dynamics, Governance and Inclusive Development, University of Amsterdam; Amsterdam, Netherlands.
[13] Department of Water Management, Delft University of Technology; Delft, Netherlands.
[14] Institute of Physical Geography, Goethe University Frankfurt; Frankfurt, Germany.
[15] Senckenberg Leibniz Biodiversity and Climate Research Centre Frankfurt (SBiK-F); Frankfurt, Germany.
[16] Institute of Engineering Hydrology and Water Resources Management, Ruhr-University Bochum; Bochum, Germany.
[17] School of Geography, University of Nottingham; Nottingham, NG7 2RD, United Kingdom.
[18] Center for Climate Change Adaptation, National Institute for Environmental Studies; Tsukuba, Japan.
[19] Moon Soul Graduate School of Future Strategy, Korea Advanced Institute of Science and Technology; Daejeon, Korea.
[20] International Institute for Applied Systems Analysis; Laxenburg, Austria.
[21] Department of Physical Geography, Utrecht University; Utrecht, Netherlands.

*Corresponding author. Email: miina.porkka@aalto.fi, vili.virkki@aalto.fi
†These authors contributed equally to this work.

Abstract

Human actions compromise the many life-supporting functions provided by the freshwater cycle. Yet, scientific understanding of anthropogenic freshwater change and its long-term evolution is limited. Using a multi-model ensemble of global hydrological models, we estimate how, over a 145-year industrial period, streamflow and soil moisture have deviated from pre-industrial baseline conditions (defined by 5^{th}–95^{th} percentiles, at 0.5° grid level and monthly time step). We find increased frequency of local deviations on ~45% of land area, mainly in regions under heavy direct or indirect human pressures. To estimate humanity's aggregate impact on the freshwater cycle, we present the evolution of deviation occurrence at regional to global scales. Currently, local streamflow and soil moisture deviations occur on 18.2% and 15.8% of global land area, respectively, which is 8.0 and 4.7 percentage points beyond the ~3 percentage point wide pre-industrial variability envelope. Finally, we discuss applying our approach to define a planetary boundary for freshwater change. Our results indicate a substantial shift from stable pre-industrial streamflow and soil moisture conditions to persistently increasing change and a transgression of the freshwater change planetary boundary, calling for urgent actions to reduce human disturbance of the freshwater cycle.

Introduction

Freshwater systems globally are under unprecedented pressure from human actions. Water extraction and infrastructure, land use and land cover change, and climate change now considerably modify the quantity and timing of atmospheric and terrestrial freshwater flows, with crucial implications for Earth's climate and ecosystems[1]. Remarkable signals of water cycle changes include widespread and severe river flow regime alterations[2], intensification[3] and homogenisation[4] of the global water cycle, and increases in the severity, frequency, and duration of floods and droughts[5].

Scientific understanding of the magnitude and nature of anthropogenic water cycle change that matters for the hydroclimatic and hydroecological stability of the Earth system is yet limited. Water cycle changes are typically analysed over relatively short time periods, typically decades[6–8]. Furthermore, changes are often quantified against reference conditions that are already affected by anthropogenic influences such as climate change (e.g. [9–11]). Studies also rarely provide global aggregation of water cycle changes that would be meaningful for assessing the state and trajectory of the global water cycle as a whole. For example, assessing change in single elements of the water cycle[2,6,11–17] or aggregating freshwater flows and stocks very broadly (whether in space[7,18,19] or in time[8,20]) may disregard the Earth system relevance of freshwater. Thus, overall, existing studies lack a long-term overarching perspective on aggregated anthropogenic water cycle change in the Earth system.

Here, we assess humanity's ever-increasing aggregate impact on the freshwater cycle, quantifying blue (represented by streamflow) and green water (represented by root-zone soil moisture – hereinafter simply soil moisture – that is the soil water available to plants) deviations from pre-industrial baseline conditions, across scales from local to global. Jointly assessing change in streamflow and soil moisture conditions, using coherent methodology, allows for inferring changes in other water cycle elements and the varying drivers of freshwater change. We define the pre-industrial period 1661–1860 as a baseline that we assume to be largely undisturbed by human impacts and assess freshwater change over the following one and a half centuries (1861–2005) against it – illustrating the trajectory of how human-driven freshwater change has evolved. Widespread deviations from the 'pristine' state that are detected by our approach can be considered to pose elevated risks to the Earth system functions of freshwater. For example, terrestrial and freshwater ecosystems have adapted to specific quantities and timing of water flows such that changes in soil moisture and streamflow can severely affect ecosystem status and biodiversity[21–23]. Moreover, the wetness of landscapes regulates climate from micro- to regional and global scales, such that changes in the magnitude and timing of wetness can impact rainfall and consequently streamflow and soil moisture both locally and remotely[24].

Our approach refines the method proposed by Wang-Erlandsson et al.[25] for quantifying a planetary boundary (PB) for green water. PBs set limits to nine processes, including freshwater use, that together regulate the state of the Earth system and thus delimit a safe operating space for retaining a quasi-stable Holocene-like state[26,27]. Previous freshwater PB estimates, which have focused on only blue water use, have been criticised for their limited capacity to capture the interconnected direct and indirect anthropogenic pressures on the water cycle[28]. Advancing the work of Wang-Erlandsson et al.[25], we present a coherent, comparable, and spatially explicit

assessment of blue (streamflow) and green water (soil moisture) change, utilising an ensemble of consistently forced global hydrological models (Fig. 1, Methods). Our approach robustly addresses criticism of previous freshwater PB definitions and quantifications. We therefore follow Wang-Erlandsson et al.[25] in proposing to use it to replace the current definition of a PB for *freshwater use* with an integrated PB for *freshwater change*.

Main

To estimate freshwater change across scales, we used streamflow and soil moisture data simulated by an ensemble of state-of-the-art gridded global hydrological models that were forced with bias-adjusted CMIP5 climate models and dynamic socio-economic conditions (Methods, Table S1). The data was given in two time periods: pre-industrial period (1661–1860) and industrial period (1861–2005).

Based on the 200-year pre-industrial period, we set the *local baseline range* (Fig. 1a) for each 0.5° grid cell and month, respectively for streamflow and soil moisture. The local baseline range is defined as the range between the 5th (*dry bound)* and the 95th (*wet bound)* percentiles of pre-industrial monthly streamflow or soil moisture values (Fig. 1a). We then compared pre-industrial streamflow and soil moisture data against the local baseline range to detect *local deviations* (Fig. 1b). Months with values below the dry bound were marked as *dry local deviations,* and months with values above the wet bound were marked as *wet local deviations* (Fig. 1b). The areas of grid cells with local streamflow or soil moisture deviations were then summed up globally (regionally). We divided this sum by total ice-free land area to yield the *percentage of land area with local deviations* (Fig. 1c). Finally, to establish global (regional) reference conditions, we defined *pre-industrial variability* (Fig. 1d) from the pre-industrial percentage of land area with local deviations. Two key metrics characterise pre-industrial variability: *the median of pre-industrial variability* and *the upper end of pre-industrial variability* (Fig. 1d). The median corresponds to the 50th and the upper end to the 95th percentile of the percentage of land area with local streamflow or soil moisture deviations during the pre-industrial period.

After defining the pre-industrial reference conditions, we compared industrial streamflow and soil moisture data against them. We repeated the detection of local deviations (Fig. 1b) and computed the percentage of land area with local deviations (Fig. 1c), which allowed us to compare changes in local deviation frequency (Fig. 1e) and in the percentage of land area with local deviations (Fig. 1f).

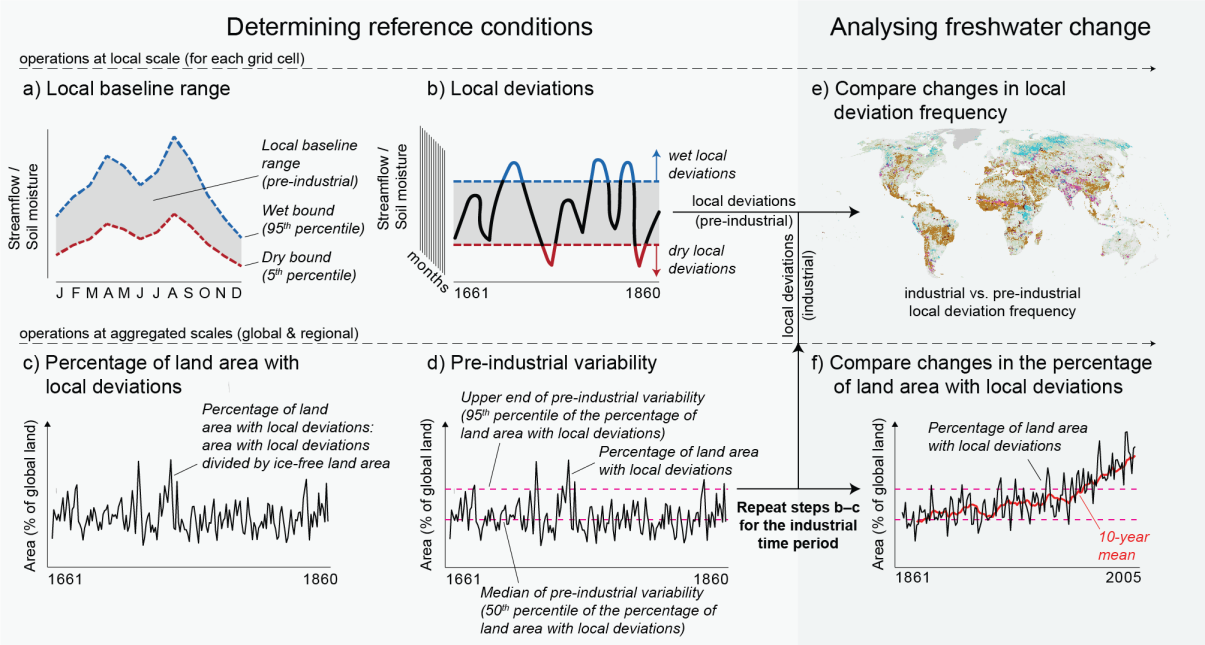

Fig. 1. Methodological outline: setting the local baseline range (a), identifying local deviations (b), computing the percentage of land area with local deviations (c), defining pre-industrial variability (d), and comparing the industrial period against the pre-industrial period (e–f). The steps a–d are described in detail in Methods.

Global freshwater change

We found no substantial changes or trends in the global land area with local streamflow or soil moisture deviations during the pre-industrial period, which indicates stable water cycle conditions prior to industrialisation (Fig. 2). The median of pre-industrial variability (i.e. the typical land area with freshwater deviations) was at 9.4% for streamflow and at 9.8% for soil moisture, respectively (Fig. 2). This is in accordance with the expectation that dry or wet deviations should each occur in 5% of the data points in each grid cell over the pre-industrial period (Methods). Annually, the pre-industrial percentage of land area with local deviations varied mostly within +/- 1.5 percentage points (pp) around the median of pre-industrial variability, and no global trends could be observed before 1860 (Fig. 2). Therefore, these relatively stable pre-industrial conditions can be considered a useful reference baseline that is not influenced by major anthropogenic impacts on the water cycle.

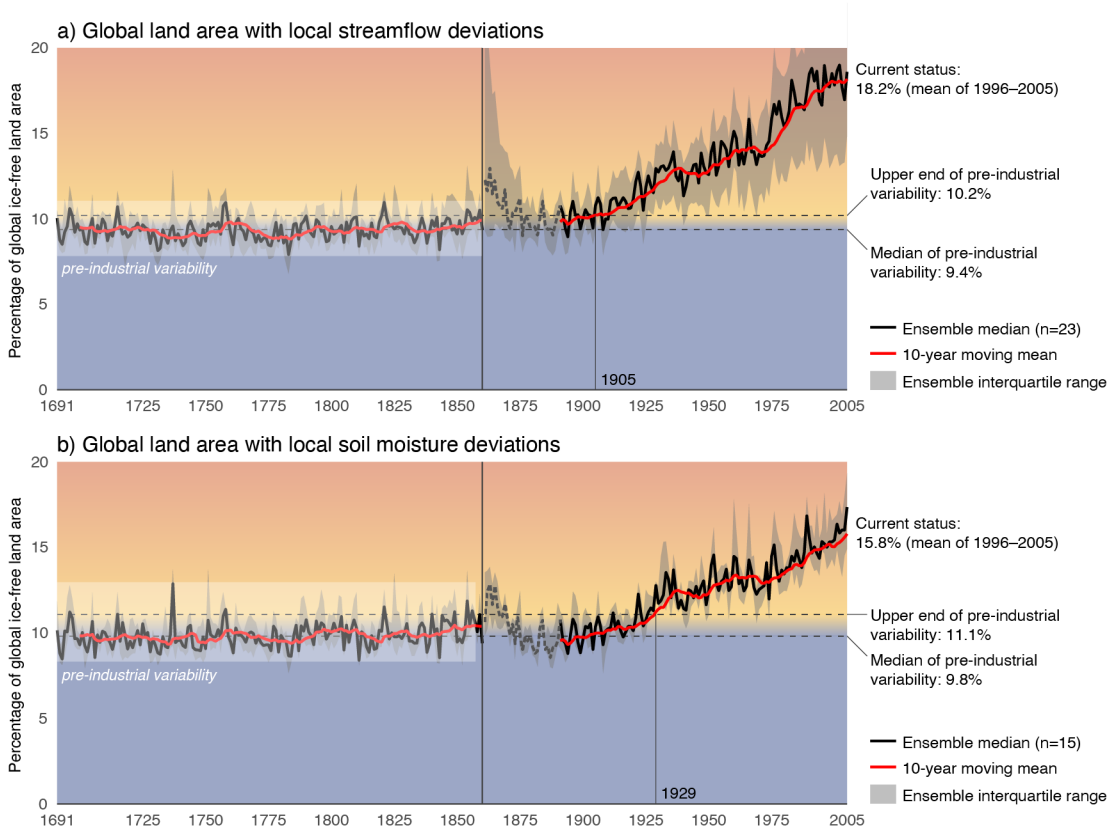

Fig. 2. Percentage of global ice-free land area with local streamflow (a) and soil moisture (b) deviations. Shown is the annual percentage, which is computed as an average of monthly percentages. The annotated years mark the 10-year moving (trailing) mean transgressing the upper end of pre-industrial variability (95th percentile of the pre-industrial percentage of land area with local deviations; Fig. 1d). The ensemble median and interquartile range are computed from n = 23 (streamflow) and n = 15 (soil moisture) ensemble members. Sensitivity analysis using different definitions of the local baseline range (Fig. 1a) is presented in Extended Data Fig. 1. Values prior to 1691 are excluded and the ensemble median line for 1861–1890 is shaded and dashed due to traces of model spinups being common during these years (Extended Data Fig. 2–3). Model-wise percentages of land area with local freshwater deviations are shown in Extended Data Fig. 4–5. Sensitivity analysis using different definitions of the local baseline range (Fig. 1a) is presented in Extended Data Fig. 1.

However, occurrence of streamflow and soil moisture deviations started to steadily increase after the end of the pre-industrial period, with both global indicators surpassing the upper end of pre-industrial variability in the early 20th century (Fig. 2). Global land area with local streamflow deviations transgressed the upper end of pre-industrial variability (10.2%) already in 1905. The degree of transgression continued to increase apart from two dips around 1940 and 1970. By the end of our study period (mean of 1996–2005), areas with local streamflow deviations covered 18.2% (~24 million km^2) of global ice-free land area (Fig. 2a). This corresponds to a 78% (8.0 pp) increase compared to the upper end and a 94% (8.8 pp) increase compared to the median of pre-industrial variability. The development of streamflow deviation occurrence is mainly due to dry deviations, which were still increasing in spatial coverage by the end of our study period, while the increase in wet deviations had plateaued decades earlier (Extended Data Fig. 6b–c).

Soil moisture exhibits a similar, though slightly less pronounced, global trajectory and pattern: the upper end of pre-industrial variability (11.1%) was transgressed in 1929, after which the land area with local soil moisture deviations increased consistently, apart from two dips (like

streamflow) in the latter half of the 20th century (Fig 2b). During the last decade (1996–2005) of our analysis period, local soil moisture deviations occurred on 15.8% (~ 20 million km^2) of global ice-free land area, which is 42% (4.7 pp) above the upper end of pre-industrial variability and 61% (6.0 pp) above its median. In contrast to streamflow, by the end of our study period, occurrence of dry soil moisture deviations was declining slowly, yet remaining at considerably higher levels than during the pre-industrial period, while occurrence of wet deviations continued to increase towards the end of the 20th century (Extended Data Fig. 6e–f).

These global patterns are robust against key methodological sensitivity. When widening the local baseline range, relative transgressions of the upper end of pre-industrial variability increase (indicating that the most extreme conditions increased more than less extreme), but, importantly, pre-industrial stability and the temporal evolution during the industrial period remain similar (Extended Data Fig. 1). In addition, though the model spread is relatively large especially towards the present day and in the case of dry streamflow deviations (Extended Data Fig. 4–6), the entire ensemble interquartile range surpasses the upper end of pre-industrial variability in the latter half of the 20th century (Fig. 2). This means that the hydrological models used here mostly agree on the evolution of the percentage of global land area with local deviations. Hence, there has been – and is still ongoing – a robust and remarkable drift away from the quasi-stable pre-industrial soil moisture and streamflow conditions (characterised by a narrow, ~3 pp wide variability range) to persistently increasing change in the freshwater cycle (currently 4.7–8.0 pp beyond pre-industrial variability).

Local and regional freshwater change

Mapping changes in the frequency of local deviations reveals a general pattern of more frequent dry deviations of both streamflow and soil moisture in much of the tropics and subtropics, with wet deviations becoming more common in temperate and subpolar regions, and in many highland areas (Fig. 3, Extended Data Fig. 7). For streamflow, increases in the frequency of dry local deviations are more common, while for soil moisture, neither dry nor wet deviation frequency increase dominates over the other. Comparing local deviation frequency in 1976–2005 against 1691–1860, 39.2% of land area shows a statistically significant increase in dry streamflow deviation frequency, while 9.2% of land area exhibits a statistically significant increase in wet streamflow deviation frequency. For soil moisture, 26.9% of land area shows an increase in dry and 19.2% an increase in wet deviation frequency. Areas in which the frequency of both dry and wet local deviations increased significantly cover 2.0% (streamflow) and 1.0% (soil moisture) of land area. Therefore, 46.4% of land area has experienced a statistically significant increase in streamflow deviation frequency and 45.1% in soil moisture deviation frequency. Increases in local deviation frequency were major (> 5 pp increase, i.e. the frequency of deviations has more than doubled compared to the expected 5% frequency) in approximately half of the area with increased frequency of dry streamflow deviations, a third of the area with increased frequency of soil moisture deviations (both dry and wet), and a quarter of the area with increased frequency of wet streamflow deviations (Fig. 3).

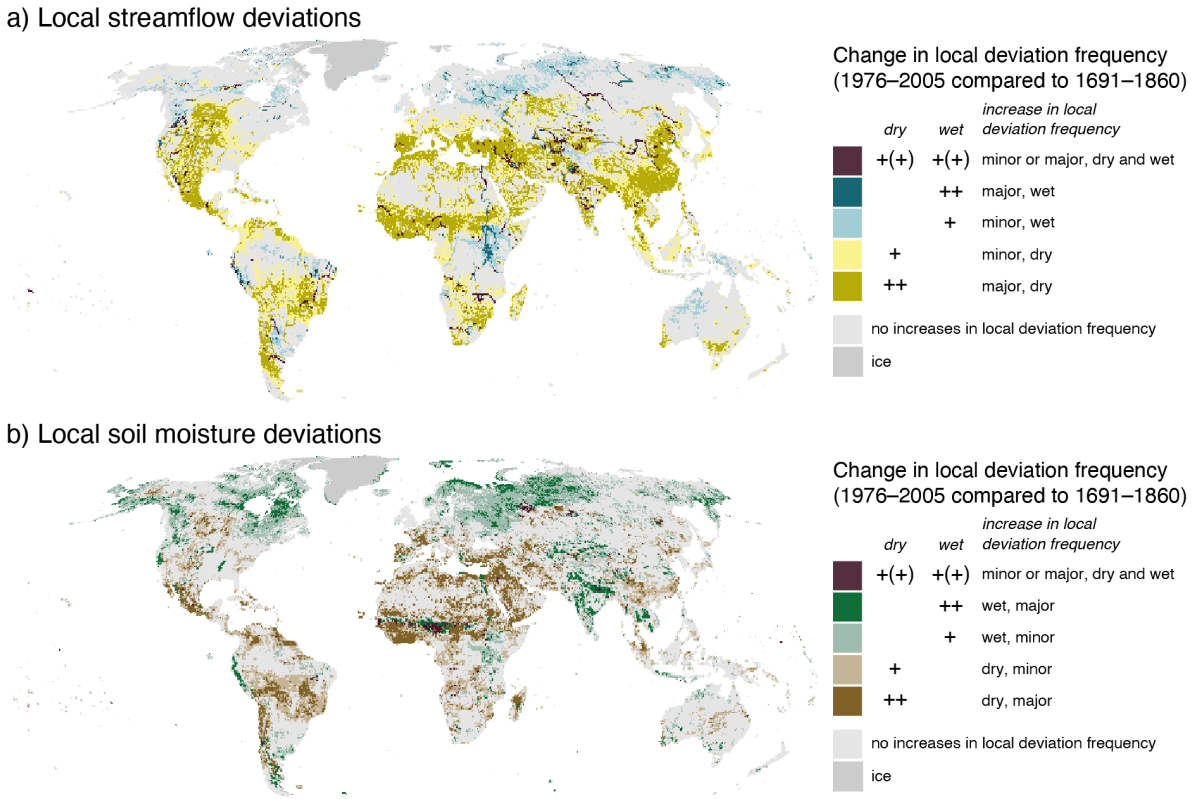

Fig. 3. Statistically significant increases in dry and wet local deviation frequency for streamflow (a) and for soil moisture (b). Changes in the frequency of local deviations are computed by comparing the ensemble median frequency of local deviations during 1976–2005 against 1691–1860, and significance of change is tested at a 95% confidence level (p = 0.05) with R package *stats* function *prop.test*[29]. Colours denoted with + indicate statistically significant increases with magnitude ≤5 pp (minor), whereas colours denoted with ++ indicate statistically significant increases with magnitude >5 pp (major). Colours denoted with +(+) pool together any statistically significant increase (minor or major).

Persistent freshwater changes and their timing are spread out unevenly (see Fig. 4, in which local freshwater deviations are aggregated at river basin scales instead of the global scale). In many regions – especially around mid-latitudes – land area with local deviations persistently transgressed the region-specific upper end of pre-industrial variability already before 1940, while in other areas – particularly in humid regions – a transgression has not occurred yet. The Mississippi, Indus, and Nile basins, for instance, were among the first regions where persistent transgression happened in case of streamflow (in the Nile, also for soil moisture) (Fig. 4a–b). For soil moisture, persistent transgression has occurred in fewer regions and often later than in the case of streamflow (Fig. 4c–d). This is visible particularly in Siberian basins, the Congo basin, and South/Southeast Asia, where the persistent transgression year for soil moisture followed 10–20 years after that of streamflow – or the transgression has not occurred yet (Fig. 4).

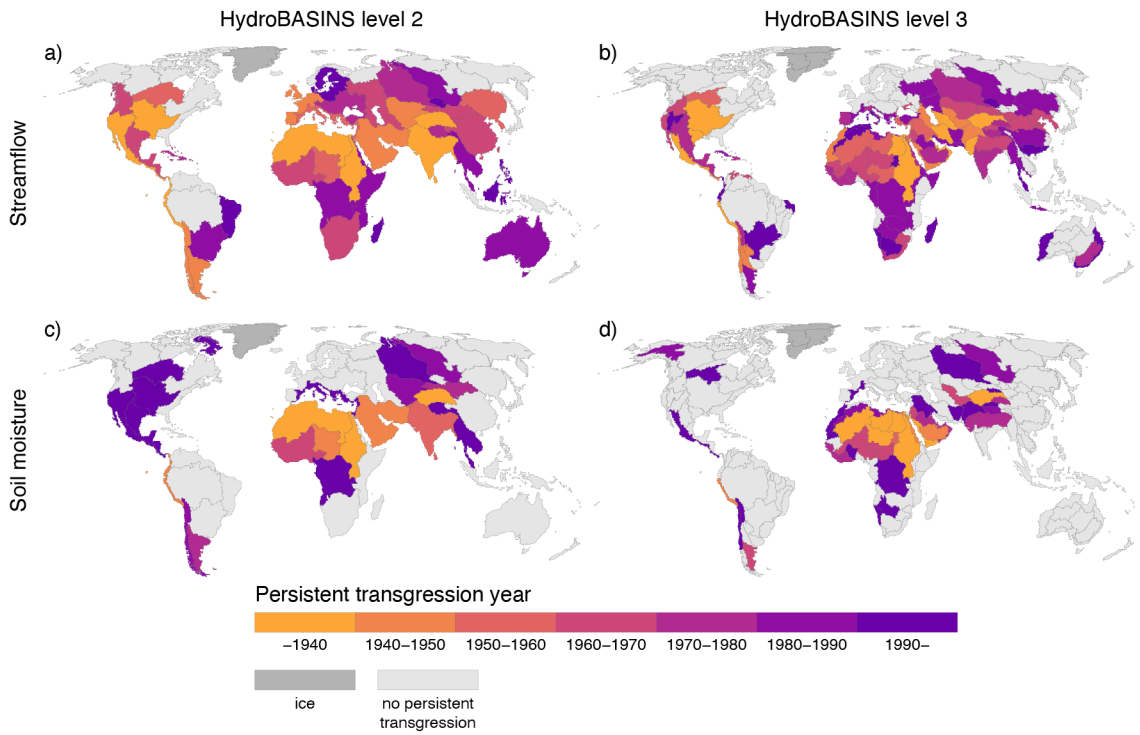

Fig. 4. Timing of persistent transgression of the region-specific upper end of pre-industrial variability, for streamflow (a–b) and soil moisture (c–d). Here, local deviations are first aggregated regionally to get pre-industrial percentage of land area with local deviations (Fig. 1c), then the upper end of pre-industrial variability is set to the 95th percentile of the percentage of land area with local deviations (Fig. 1d), and finally the percentage of land area with local deviations is calculated for the industrial period and compared against pre-industrial variability (Fig. 1f). The persistent transgression year is defined as the first year, during which the 10-year moving (trailing) mean of percentage of land area with local deviations has exceeded the region-specific upper end of pre-industrial variability for ten consecutive years, without returning below this limit after this year. The regions shown here depict basins delineated by the HydroBASINS data set level 2 (a, c; n = 60, mean area = 2,247,000 km^2, median area = 2,045,000 km^2) and level 3 (b, d; n = 264, mean area = 511,000 km^2 median area = 313,000 km^2)[30].

Drivers and impacts of freshwater change

Assessing the changes in local streamflow and soil moisture deviations in unison provides more detailed insights into their causes and potential impacts. The general pattern of increasing wet deviation frequency of both streamflow and soil moisture in the Northern Hemisphere likely arises from the precipitation change due to ~1°C of mean global warming[5], which affects both streamflow and soil moisture similarly if major human impacts on land surface, such as land cover change and soil degradation, do not change precipitation partitioning. Another distinctive example of climate-induced deviations is the Sahel region (stretching across the African continent south of the Sahara; partially covered by the Niger river basin in Fig. 5). Drier conditions (relative to pre-industrial climate) dominated in the region already in the first half of the 20th century[31] – which agrees with our analysis showing increased dry deviation frequency already when comparing 1931–1960 against 1691–1860 (Extended Data Fig. 8) – and intensified from the 1970s onwards. Recent decades have additionally witnessed widespread wet local deviations (and different combinations of dry and wet), which could be explained by changes in temporal dynamics, such as intensity of precipitation, number of wet days, occurrence of dry spells and timing and length of the rainy season[31,32].

As an example of direct human drivers, increased frequency of dry local streamflow deviations in combination with wet local soil moisture deviations in a given area most likely indicates an effect of irrigation expansion. Indeed, these cases are observed in many heavily irrigated regions[33], such as South Asia, eastern China, Western USA, and the Nile delta (Fig. 5, pink colour). These regions are also the likely early drivers of globally aggregated deviations, as their irrigation extent was relatively large already in the early 20th century[33], and local deviations were prevalent already then (Extended Data Fig. 8). Increases in the frequency of both wet and dry streamflow deviations, as well as wet soil moisture deviations, (Fig. 5, dark blue) could imply a situation in which the natural river flow regime has been altered by dam operation (decreased flood peaks and increased dry season streamflow) in combination with extensive irrigation (decreased streamflow, increased soil moisture). These cases can be found in many heavily modified river basins[34], such as the Nile, the Aral Sea, and parts of India and Thailand (Fig. 5).

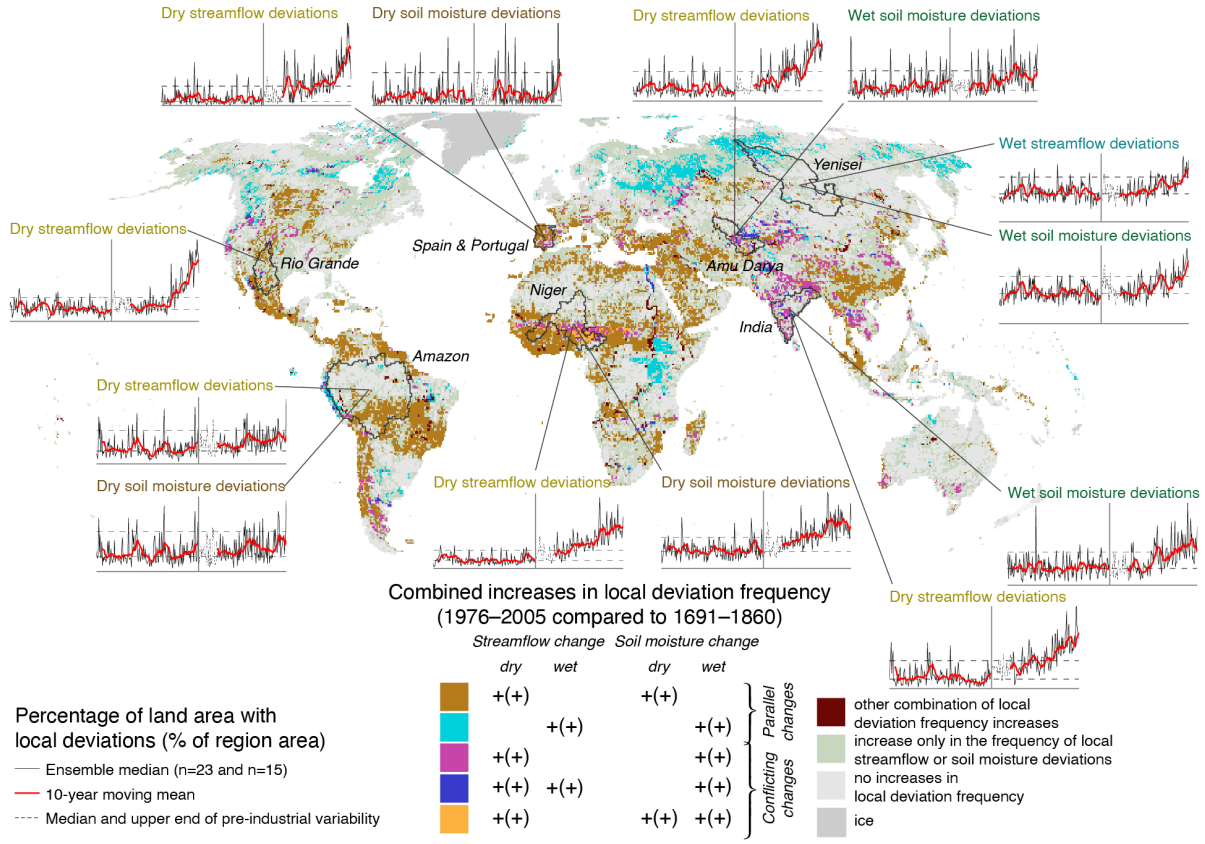

Fig. 5. Combined increases in local streamflow and soil moisture deviation frequency along with regional percentages of land area with dry or wet local deviations in selected regions. The classification is based on local deviation frequency increases presented in Fig. 3, and it pools together both minor and major increases (represented by +(+) in the legend). Computing the percentage of land area with local deviations (Fig. 1c) was performed within each region, and the median and upper end of pre-industrial variability (Fig. 1d) were also computed regionally.

Our findings of increased streamflow and soil moisture deviation frequency are consistent with many regional to global freshwater-mediated impacts that have been reported independently. One of the most dramatic examples of blue water change is the Aral Sea, where the anthropogenic overuse of water for irrigation resulted in a massive lake depletion, consequent ecological degradation, and regional climate change[35]. In our results, the region's two large river basins, Amu Darya and Syr Darya, exhibit a steep increase in dry streamflow and a

moderate increase in wet soil moisture deviations, starting in the late 1960s (Fig. 5) – in accordance with the substantial irrigation expansion that started in the region at that time[35].

Soil moisture changes have been associated with productivity loss, as exemplified by drying-induced forest dieback[36] in many of the regions where we find a major frequency increase in dry soil moisture deviations, such as the Mediterranean basin, central North America and West Africa (e.g. Niger river basin in Fig. 5). Productivity shocks due to dry and wet soil moisture deviations (droughts and floods) have also been reported on many cultivated lands, particularly in South and East Asia, Australia, and North Africa[37], where we find both drying and wetting (Fig. 3b, India in Fig. 5). Other examples of ecological and climatic impacts of water surpluses are habitat loss in the Central Amazon floodplains due to anthropogenic flood pulse disturbance by dams[38], and increased greenhouse gas emissions from reservoirs[39], though these freshwater alterations are relatively small-scale and thus not clearly visible in our maps.

Introducing the new planetary boundary for freshwater change

The existing freshwater planetary boundary estimates have fallen short in capturing freshwater change due to e.g. land use and land cover change, and anthropogenic greenhouse gas and aerosol emissions, which alter evaporation, soil moisture, precipitation and runoff patterns[28,40–44]. Existing approaches have also been criticised for aggregating freshwater fluxes too broadly, e.g. by operating on an annual scale only or simply summing global water use and availability despite diverse local impacts[45,46]. These simplifications may conceal important variation across space and time and overlook, or cancel out, the often-contrasting impacts of human drivers on different parts of the water cycle. For example, irrigation decreases streamflow but increases soil moisture, and hydropower operations increase evaporation by reservoir impoundment, as well as shift water flows temporally from the wet to the dry season and blue water scarcity hotspots from upstream to downstream[47]. Therefore, the narrow and one-dimensional outlook on freshwater change by the existing freshwater PB estimates is due for a more comprehensive replacement.

Following Wang-Erlandsson et al.[25], we argue that our approach and results are fitting to be used in setting a new PB for freshwater *change* (as opposed to the current PB for freshwater *use*) because we can capture global water cycle change by analysing several of its components, using metrics that relate to its Earth system impacts, and adopting meaningful (Holocene-like) baselines and long time scales. Although streamflow and soil moisture represent only a part of the freshwater cycle, they are connected, either directly or indirectly, to all major anthropogenic modifications of the freshwater cycle and associated Earth system functions (SI text).

We propose the upper end (95th percentile) of pre-industrial variability in global land area with local streamflow (blue water) and soil moisture (green water) deviations as the two components of the PB for freshwater change. This definition represents global conditions occurring expectedly once in 20 years in the pre-industrial reference state and corresponds to 10.2% of the global land area for blue water (Fig. 2a) and 11.1% for green water (Fig. 2b). This boundary placement assumes that widespread deviations from pre-industrial conditions (which represent longer-term Holocene-like conditions) pose elevated risks to freshwater's Earth system functions. According to our results, the freshwater change PB has been transgressed for a long time – the current status is 18.2% for the blue and 15.8% for the green water component (Fig. 2). This is in stark contrast with the key PB publications' estimates of the freshwater use PB's

safe status[27,48] but agrees with other, more nuanced studies on the freshwater use PB[18,49], which consider the boundary to be transgressed.

It should be noted that there are major uncertainties associated with setting the freshwater change PB (Methods, SI text). While data-related uncertainties have been mitigated by using a large ensemble of state-of-the-art global hydrological models that have been validated against observations[50–53], perhaps the most important uncertainty stems from the lack of robust quantifications of Earth system-wide responses to water cycle modifications that surpass pre-industrial variability. These responses may be too complex to be quantified with our current knowledge, and it is also possible that the level of freshwater modifications that drives state changes and increases risks in the Earth system can only be determined in retrospect.

Nevertheless, because the freshwater cycle upkeeps many life-supporting Earth system functions, risks of environmental degradation can be assumed to elevate along with change away from a stable, Holocene-like state[1] – a change that has occurred in the freshwater cycle within the last century (Fig. 2). While it is possible that buffers or stabilising feedbacks (such as CO_2 fertilisation) in the Earth system allow for increased variability in the water cycle (such as for the currently observed change), there is also evidence that self-reinforcing feedbacks (such as forest dieback and moisture recycling feedbacks[54]) may amplify the impacts of freshwater change on Earth system functioning. Considering also freshwater's central role in Earth system process interactions[55], the precautionary principle of the PB framework[48] thus motivates a conservative placement of the new PB for freshwater change at the lower level of scientific uncertainty. Here, we consider this to be the upper end of pre-industrial variability. The major transgression and remaining uncertainties of this boundary placement, however, warrant continued research on the role of freshwater in the Earth system.

Concluding remarks

We have presented here the trajectory of anthropogenically driven freshwater change since the stable pre-industrial period and shown that this change has been pervasive across spatial and temporal scales. Globally, land area in which streamflow and soil moisture deviates from local pre-industrial reference conditions has increased by 78–94% and 42–61%, respectively, within the 145-year industrial period. This major shift in the global water cycle is in accordance with the few other studies reporting long-term (>100 years) changes, such as groundwater depletion of at least ~4,500 km^3, corresponding to >6% of total sea-level rise[16] (and possibly much greater[15]), and at least a 21% loss of wetlands since the year 1700[13,14]. Our results align well also with studies reporting decadal changes and trends in increasing hydrological extremes[5]. Locally, evidence of freshwater-triggered ecological and climatic shifts has been mounting as the main components of the freshwater cycle have moved further away from their pre-industrial variability. Our findings indicate a transgression of the planetary boundary for freshwater change already around the mid-20th century, while climate change[56], deforestation[57] and many other human pressures on the water cycle continue to pose a major risk of further change. Decreasing these pressures are thus imperative to reducing human disturbance of the water cycle and to avoiding compromising the life-supporting functions of freshwater.

Methods

Data selection

Our main data source was the Inter-Sectoral Impact Model Intercomparison Project (ISIMIP) data repository (available at: https://data.isimip.org, last accessed March 30th, 2023), from which we used data of the ISIMIP 2b simulation round[58] experiments (Table S1). We used root-zone soil moisture (hereinafter soil moisture; ISIMIP output variable *rootmoist*) to represent green water and river discharge (hereinafter streamflow; ISIMIP output variable *dis*) to represent blue water as the two main components of the freshwater cycle. The models in ISIMIP 2b have been validated against observations, showing adequate performance especially when estimates from individual models are combined in an ensemble modelling approach[50–53]. By constructing ensembles as large as possible, given the availability of different simulation scenarios, we can partially tackle the uncertainty to which global modelling is always subject to, to a certain degree[59].

Two distinct simulation scenarios were required to determine the pre-industrial reference state (Fig. 1a–d) and compare the industrial and pre-industrial states of the water cycle (Fig. 1e–f). For the pre-industrial period (1661–1860), we used model outputs forced with *picontrol* climate and *1860soc* land use and socio-economic conditions, which described our pre-industrial reference state with a constant 286 ppm CO_2 concentration and fixed pre-industrial land use and socio-economic conditions[58]. The pre-industrial simulation years are, however, nominal, as the CMIP5 data used to force ISIMIP 2b models represent 200 control years with climate variability at pre-industrial levels (with no correspondence to the actual weather of individual years)[58]. At the transition from pre-industrial to industrial time (as defined by the ISIMIP protocol) in 1860, we switched to *historical* climate combined with *histsoc* land use and socio-economic conditions, in which carbon-induced climate change and human influences (e.g. land use change, water use, and dam operation) were dynamically represented in the data[58]. The ISIMIP 2b industrial period covers years from 1861 to 2005, the end year owing to estimates of e.g. irrigation extent not being available[33].

In ISIMIP 2b, soil moisture and streamflow were simulated by global hydrological models (GHMs), which were forced with bias-adjusted output of modelled climate from general circulation models (GCMs). The GCM outputs from CMIP5 models[60] were bias-adjusted with an observational dataset covering the years 1979–2013[58]. We selected all GHM-GCM combinations, for which output data were available for both *picontrol-1860soc* and *historical-histsoc* scenarios (Table S1). For soil moisture, outputs from four GHMs (CLM50[61], LPJmL[62], MPI-HM[63], and PCR-GLOBWB[64]) were available, and for streamflow, outputs from six GHMs (H08[65], LPJmL, MATSIRO[66], MPI-HM, PCR-GLOBWB, and WaterGAP2[67]) were available. For all GHMs, outputs of four GCMs were available: GFDL-ESM2M[68], HadGEM2-ES[69], IPSL-CM5A-LR[70], and MIROC5[71], except for MPI-HM, which lacked data forced with HadGEM2-ES for both streamflow and soil moisture. Hence, our soil moisture data ensemble consisted of 15 members (GHM-GCM combinations) and our streamflow data ensemble consisted of 23 members. For streamflow, we aggregated daily values to monthly values by taking the mean of daily streamflow, whereas soil moisture data were readily delivered in monthly time resolution. The spatial resolution of all data was 0.5 degrees (ca. 50 x 50 km at the Equator).

Data preparation

Because the data we used originated from two different scenarios, and the ISIMIP simulations can be run independently of each other, the outcomes of the two scenarios may not be continuous (i.e. the end state of the pre-industrial simulation does not necessarily equal the initial state of the industrial simulation at the grid cell scale). Two kinds of discontinuities may therefore arise: 1) traces of model spinup, with GHMs reaching a water storage equilibrium with delay at the beginning of the simulation, and 2) abrupt shifts in value distribution around the transition point at the end of year 1860 (e.g. in the moving mean). Further, a combination of the two is also possible. Thus, we ensured that the simulation outcomes were harmonious with a two-step approach applied separately for each grid cell, month, and ensemble member. Extended Data Fig. 2 shows an example of traces of model spinup, whereas Extended Data Fig. 3 shows our general approach to ensure the fit between the simulation periods along with an example of a cell in which the value distribution shifts.

First, we checked for any traces of spinups by detecting the most likely changepoint in the mean and variance of the data with function *cpt.meanvar* in R package *changepoint*[72,73], separately for the pre-industrial and industrial periods. As the trace of spinup is related to reaching an equilibrium in the hydrological state in a cell, we assumed that a true trace of spinup is located between 10 and 30 years after the initiation of each simulation period. Outside this period, we considered that detected changepoints were true (natural) changes in mean and variance and did not imply a trace of spinup in the data. If a changepoint was detected between 10 and 30 years after initiation (as in Extended Data Fig. 2, for example), all data before the changepoint were excluded from distribution shift correction; otherwise (as in Extended Data Fig. 3, for example), data from the ten first years of the simulation periods were discarded. Depending on the month and ensemble member, changepoints indicating traces of spinup were detected in 1.4–8.7% (pre-industrial streamflow), 1.6–7.2% (industrial streamflow) 0.4–4.6% (pre-industrial soil moisture), and 0.6–5.7% (industrial soil moisture) of all cells.

Second, we checked and corrected shifts in value distribution around the simulations' transition point in 1860, using an iterative technique combining linear extrapolation and quantile mapping. Because the simulation periods have no temporal overlap, we extrapolated pre-industrial data onto the industrial simulation period (i.e. extended the pre-industrial time series to nominally cover years past 1860). This was done by fitting a linear regression model[74] to pre-industrial values excluding spinup (i.e. 1671–1860 in most cases, with flexibility of starting from 1691 at latest), and extrapolating the detected linear trend to the industrial period (blue lines in Extended Data Fig. 3a). Further, we computed the standard deviation of the pre-industrial values to which the linear model was fit (defined here as σ_{preind}) and added normally distributed random noise ($\mu = 0$, $\sigma = \sigma_{preind}$) around the linear extrapolation line to create extrapolated data points (blue circles in Extended Data Fig. 3a).

After extrapolation, we fitted non-parametric quantile mapping using robust empirical quantiles implemented in R package *qmap*[75,76] between the industrial simulation values and the values that were extrapolated from the pre-industrial period to cover the first years of the industrial simulation period. Four quantiles were used in fitting the quantile mapping. Here, we treated the industrial simulation values as 'observed' data and the extrapolated pre-industrial values as 'modelled' data, although both were simulated GHM outputs. We chose to fit the quantile mapping between 30 years of industrial and extrapolated pre-industrial values, starting

from the first year not excluded after spinup detection (pink shading in Extended Data Fig. 3a). Hence, quantile mapping was mostly fitted using years 1871–1900 as the 'observed' values but with flexibility of extending the fitting period to 1891–1920 at maximum. For example, the fitting period for the cell shown in Extended Data Fig. 2 was 1874–1903, whereas for the cell shown in Extended Data Fig. 3, the fitting period was 1871–1900. Although 30 years is a relatively short period, and some spinups might end only after 1891, we chose to limit the quantile mapping with these years to prevent the industrial values being substantially affected by anthropogenic impacts, which becomes more likely during the 20th century.

Finally, pre-industrial values excluding spinup were corrected with the fitted quantile mapping function (Extended Data Fig. 3b). However, as our correction procedure included extrapolation and had a relatively small sample size (of 30), distinctive individual values or undetected traces of spinup might have distorted the quantile mapping function. Hence, we checked whether applying quantile mapping succeeded in improving the fit between the simulation periods. To do this, we ran our analysis up until detecting local deviations (Fig. 1a–b) – first without correction and then with correction – and consequently checked whether the number of local deviations (Fig. 1b) decreased owing to the correction. Checking the local deviations was performed for a period of 50 years, beginning from the first year not excluded after spinup detection (hatched fill in Extended Data Fig. 3). This was to include data outside the period that was used in fitting the quantile mapping. If the number of local deviations decreased, we considered that our correction procedure had improved the fit between the simulation periods and the corrected cell values were accepted, otherwise we discarded the corrected data and retained the uncorrected data. Globally, depending on month and ensemble member, the correction was accepted for approximately 6–26% of streamflow cells and 10–29% of soil moisture cells.

Setting the local baseline range and identifying local deviations

In setting the local baseline range (Fig. 1a), identifying local deviations (Fig. 1b), and computing the percentage of land area with local deviations (Fig. 1c), we followed the general approach of Wang-Erlandsson et al.[25] with some modifications. Like them, we set the 5th and 95th percentiles of pre-industrial streamflow and soil moisture to bound the local baseline range (separately for each grid cell, month, and ensemble member), but we drew these bounds from the considered grid cell's values only, whereas Wang-Erlandsson et al.[25] drew their local baseline range from the values in the considered grid cell and its neighbourhood. We chose a stricter definition of the local baseline range because including neighbourhood values in determining the local baseline range can potentially set it unrealistically wide – especially in the case of streamflow, in which neighbourhood values strongly depend on flow directions.

Spinups were excluded from setting the local baseline range, which means that for most cells, dry and wet bounds (Fig. 1a) were drawn from 190 values covering years 1671–1860, though allowing flexibility up until 1691 (e.g. for the grid cell shown in Extended Data Fig. 2, the bounds were drawn from values in 1690–1860). We also evaluated the sensitivity of our results to the definition of the local baseline range by repeating our main global analysis (Fig. 2) using the 2.5th and 97.5th and the 1st and 99th percentiles as the dry and wet bounds, in addition to the 5th and 95th percentiles (Extended Data Fig. 1).

Then, again for each grid cell, month, and ensemble member, we checked for all pre-industrial months whether streamflow or soil moisture would fall within or outside the local baseline range, to identify local deviations (Fig. 1b). In case a monthly value was lower than the dry bound (5^{th} percentile of pre-industrial values), this month was marked as a dry local deviation. Contrarily, in cases of the monthly value surpassing the wet bound (95^{th} percentile of pre-industrial values), the month was marked as a wet local deviation. Local deviations were evaluated for all months including spinups, and all deviations were determined in a binary fashion, as 'deviated' or 'not deviated', with no regards to deviation magnitude.

Computing the percentage of land area with local deviations and defining pre-industrial variability

After identifying local deviations (Fig. 1b), we summed up the land areas of grid cells with dry and wet local deviations, separately for each month and ensemble member. We excluded Antarctica and other permanent land ice areas using HYDE 3.2.1 anthromes[77] and divided the land area with local deviations by total ice-free land area to yield the percentage of land area with local deviations (Fig. 1c). We transformed monthly percentages into annual percentages by taking annual means of the monthly percentages. This differs from Wang-Erlandsson et al.[25] who marked an individual grid cell as deviating during a given year if a local deviation occurred in any month of that year, and subsequently computed the global percentage of land area with local deviations only annually. We chose to compute the percentage of land area with local deviations at a monthly time step to distinguish between cases in which local deviations occur in only one month or many months within a year – i.e. when freshwater change is temporally less or more extensive. With our approach, local deviations that spread out over multiple months of the year have a higher impact on the annual percentage of land area with local deviations.

As approximately 5% of all pre-industrial values in each grid cell were marked as dry and wet local deviations by the definition of the local baseline range (5^{th}/95^{th} percentiles), the expected global percentage of land area with local deviations was also approximately 5%, for dry and wet deviations separately (under conditions with little interannual variance, i.e. not during spinups). Hence, summing the percentages of land area with dry and wet local deviations together, the expected value for the global percentage of land area with local deviations was approximately 10%. As spinups were prevalent especially in some GHMs (Extended Data Fig. 4–5), global percentages of land area with local deviations prior to 1691 were excluded from further analysis. Therefore, we ended up with a time series of n = 170 for the annual pre-industrial percentage of land area with local deviations.

The pre-industrial percentage of land area with local deviations (Fig. 1c) was further used to define pre-industrial variability (Fig. 1d). In the main results, we took the ensemble median (n = 15 or n = 23) of the percentage of land area with local deviations to define two main metrics: the median of pre-industrial variability and the upper end of pre-industrial variability (Fig. 1d). The median of pre-industrial variability was defined as the 50^{th} percentile of the percentage of land area with local deviations, while the upper end of pre-industrial variability was defined as the 95^{th} percentile of the percentage of land area with local deviations. Hence, the median describes the typical percentage of land area with local deviations in the pre-industrial

(Holocene-like; presumably natural) reference state, whereas the upper end describes conditions that occur expectedly once in every 20 years.

To assess the industrial (1861–2005) state of the freshwater cycle, we repeated the identification of local deviations (Fig. 1b), computed the percentage of land area with local deviations (Fig. 1c), and compared that to pre-industrial variability (Fig. 1d). Again, we included all years in identifying local deviations, but chose to draw years 1861–1890 as shaded and dashed in the presented results, owing to spinups being prevalent in some GHMs (Extended Data Fig. 4–5). We took the ensemble median of the global percentage of land area with local deviations also for the industrial period and applied a moving (trailing) 10-year mean over this ensemble median time series, with the latest 10-year mean (for year 2005, computed as a mean of values from 1996–2005) being defined as the current status.

Limitations and uncertainties

Global hydrological models (GHMs) are known to be relatively sensitive to their internal implementation of anthropogenic drivers and impacts[51,59]. ISIMIP 2b simulations attempt to minimise uncertainties stemming from this by using state-of-the-art input data and consistent scenario definitions[58]. Nevertheless, the different process descriptions of GHMs lead to a considerable spread in our results (Extended Data Fig. 4–5), which means that our global – and especially local – results are subject to noteworthy uncertainty. We also found relatively prevalent discontinuities in the data, which we corrected for the purposes of this analysis (Extended Data Fig. 3). However, we chose not to perform an explicit validation for our hydrological data because ISIMIP 2b data has shown adequate[50–53] (though variable[78]) performance against observations, observed data to validate pre-industrial values are unavailable, and the ISIMIP 2b hydrological data used here is forced by GCM outputs instead of observed climate. We thus consider that using a data ensemble as large as possible captures the uncertainty of global hydrological modelling adequately. Moreover, our estimate of the 'current' status ends in 2005, due to the ISIMIP 2b simulation protocol[58]. Since the end of our study period, global trends in many of the key drivers of freshwater change, such as irrigated area[79], water use[80], dam construction[81] and forest loss[82], have increased, and therefore, the results presented here are likely conservative.

As our scenario setup of using dynamic *histsoc* socio-economic conditions against static *1860soc* (Table S1) already implies a change in anthropogenic drivers of water cycle change, it is not an unexpected result that aggregate water cycle changes were manifested in the early 20th century (Fig. 2, Fig. 4, Extended Data Fig. 8). Repeating the analysis using data that are absent of anthropogenic forcing (ISIMIP *nosoc* scenarios[58]) would potentially aid in estimating how large proportions of freshwater change are due to direct (e.g. water use) or indirect (e.g. climate change) anthropogenic factors. However, model outputs for both *picontrol-1860soc* (or *picontrol-nosoc*) and *historical-nosoc* scenarios were not available in ISIMIP 2b. Future modelling efforts (e.g. ISIMIP simulation round 3[83]) could provide an excellent opening to further develop our analysis.

Despite the related uncertainties, our approach is as coherent as current knowledge and modelling capacities allow for a global study. Moreover, the magnitude and rate of global freshwater change in the industrial period and the presumably conservative estimation of its

current status suggest that our conclusion of the freshwater cycle substantially transgressing its pre-industrial variability is valid.

Data availability

All data used in this study are gathered from openly available sources, which are appropriately cited in Methods. Aggregated output data produced by our analysis will be deposited in a public database and released upon publication.

Code availability

The code used in producing the results shown in this study will be deposited in a public database and released upon publication.

References

1. Gleeson, T. *et al.* Illuminating water cycle modifications and Earth system resilience in the Anthropocene. *Water Resour. Res.* **56**, e2019WR024957 (2020).
2. Virkki, V. *et al.* Globally widespread and increasing violations of environmental flow envelopes. *Hydrol. Earth Syst. Sci.* **26**, 3315–3336 (2022).
3. Huntington, T. G. Evidence for intensification of the global water cycle: Review and synthesis. *J. Hydrol.* **319**, 83–95 (2006).
4. Levia, D. F. *et al.* Homogenization of the terrestrial water cycle. *Nat. Geosci.* **13**, 656–658 (2020).
5. Douville, H., et *al*. In Climate Change 2021: The Physical Science Basis. *Contribution of Working Group I to the Sixth Assessment Report of the Intergovernmental Panel on Climate Change*. Chapter 8: Water Cycle Changes (Cambridge University Press, Cambridge, United Kingdom, 2021).
6. Gudmundsson, L. *et al.* Globally observed trends in mean and extreme river flow attributed to climate change. *Science* **371**, 1159–1162 (2021).
7. Robertson, F. R. *et al.* Consistency of Estimated Global Water Cycle Variations over the Satellite Era. *J. Clim.* **27**, 6135–6154 (2014).
8. Zhang, Y. *et al.* Multi-decadal trends in global terrestrial evapotranspiration and its components. *Sci. Rep.* **6**, 19124 (2016).
9. Haddeland, I. *et al.* Global water resources affected by human interventions and climate change. *Proc. Natl. Acad. Sci.* **111**, 3251–3256 (2014).
10. Jägermeyr, J., Pastor, A., Biemans, H. & Gerten, D. Reconciling irrigated food production with environmental flows for Sustainable Development Goals implementation. *Nat. Commun.* **8**, 15900 (2017).
11. Pastor, A. V. *et al.* Understanding the transgression of global and regional freshwater planetary boundaries. *Philos. Trans. R. Soc. Math. Phys. Eng. Sci.* **380**, 20210294 (2022).
12. Cooley, S. W., Ryan, J. C. & Smith, L. C. Human alteration of global surface water storage variability. *Nature* **591**, 78–81 (2021).
13. Davidson, N. C. How much wetland has the world lost? Long-term and recent trends in global wetland area. *Mar. Freshw. Res.* **65**, 934 (2014).
14. Fluet-Chouinard, E. *et al.* Extensive global wetland loss over the past three centuries. *Nature* **614**, 281–286 (2023).
15. de Graaf, I. E. M. *et al.* A global-scale two-layer transient groundwater model: Development and application to groundwater depletion. *Adv. Water Resour.* **102**, 53–67 (2017).
16. Konikow, L. F. Contribution of global groundwater depletion since 1900 to sea-level rise. *Geophys. Res. Lett.* **38**, (2011).

17. Grill, G. *et al.* Mapping the world's free-flowing rivers. *Nature* **569**, 215–221 (2019).
18. Jaramillo, F. & Destouni, G. Local flow regulation and irrigation raise global human water consumption and footprint. *Science* **350**, 1248–1251 (2015).
19. Adler, R. F., Gu, G., Sapiano, M., Wang, J.-J. & Huffman, G. J. Global Precipitation: Means, Variations and Trends During the Satellite Era (1979–2014). *Surv. Geophys.* **38**, 679–699 (2017).
20. Ukkola, A. M. & Prentice, I. C. A worldwide analysis of trends in water-balance evapotranspiration. *Hydrol. Earth Syst. Sci.* **17**, 4177–4187 (2013).
21. Berdugo, M. *et al.* Global ecosystem thresholds driven by aridity. *Science* **367**, 787–790 (2020).
22. Meir, P. *et al.* Threshold Responses to Soil Moisture Deficit by Trees and Soil in Tropical Rain Forests: Insights from Field Experiments. *BioScience* **65**, 882–892 (2015).
23. Richter, B., Baumgartner, J., Wigington, R. & Braun, D. How much water does a river need? *Freshw. Biol.* **37**, 231–249 (1997).
24. Wang-Erlandsson, L. *et al.* Remote land use impacts on river flows through atmospheric teleconnections. *Hydrol. Earth Syst. Sci.* **22**, 4311–4328 (2018).
25. Wang-Erlandsson, L. *et al.* A planetary boundary for green water. *Nat. Rev. Earth Environ.* **3**, 380–392 (2022).
26. Rockström, J. *et al.* A safe operating space for humanity. *Nature* **461**, 472–475 (2009).
27. Steffen, W. *et al.* Planetary boundaries: Guiding human development on a changing planet. *Science* **347**, 1259855 (2015).
28. Gleeson, T. *et al.* The Water Planetary Boundary: Interrogation and Revision. *One Earth* **2**, 223–234 (2020).
29. R Core Team. *R: A language and environment for statistical computing*. (R Foundation for Statistical Computing, 2021).
30. Lehner, B. & Grill, G. Global river hydrography and network routing: baseline data and new approaches to study the world's large river systems. *Hydrol. Process.* **27**, 2171–2186 (2013).
31. Biasutti, M. Rainfall trends in the African Sahel: Characteristics, processes, and causes. *WIREs Clim. Change* **10**, e591 (2019).
32. Porkka, M. *et al.* Is wetter better? Exploring agriculturally-relevant rainfall characteristics over four decades in the Sahel. *Environ. Res. Lett.* **16**, 035002 (2021).
33. Siebert, S. *et al.* A global data set of the extent of irrigated land from 1900 to 2005. *Hydrol. Earth Syst. Sci.* **19**, 1521–1545 (2015).
34. Lehner, B. *et al.* High-resolution mapping of the world's reservoirs and dams for sustainable river-flow management. *Front. Ecol. Environ.* **9**, 494–502 (2011).
35. Micklin, P. The Aral Sea disaster. *Annu Rev Earth Planet Sci* **35**, 47–7272 (2007).

36. Hammond, W. M. *et al.* Global field observations of tree die-off reveal hotter-drought fingerprint for Earth's forests. *Nat. Commun.* **13**, 1761 (2022).
37. Cottrell, R. S. *et al.* Food production shocks across land and sea. *Nat. Sustain.* **2**, 130–137 (2019).
38. Schöngart, J. *et al.* The shadow of the Balbina dam: A synthesis of over 35 years of downstream impacts on floodplain forests in Central Amazonia. *Aquat. Conserv. Mar. Freshw. Ecosyst.* **31**, 1117–1135 (2021).
39. Deemer, B. R. *et al.* Greenhouse Gas Emissions from Reservoir Water Surfaces: A New Global Synthesis. *BioScience* **66**, 949–964 (2016).
40. Lawrence, D. & Vandecar, K. Effects of tropical deforestation on climate and agriculture. *Nat. Clim. Change* **5**, 27–36 (2015).
41. Liu, J., Wang, B., Cane, M. A., Yim, S.-Y. & Lee, J.-Y. Divergent global precipitation changes induced by natural versus anthropogenic forcing. *Nature* **493**, 656–659 (2013).
42. Puma, M. J. & Cook, B. I. Effects of irrigation on global climate during the 20th century. *J. Geophys. Res. Atmospheres* **115**, (2010).
43. Sillmann, J. *et al.* Extreme wet and dry conditions affected differently by greenhouse gases and aerosols. *Npj Clim. Atmospheric Sci.* **2**, 1–7 (2019).
44. Sterling, S. M., Ducharne, A. & Polcher, J. The impact of global land-cover change on the terrestrial water cycle. *Nat. Clim. Change* **3**, 385–390 (2013).
45. Heistermann, M. HESS Opinions: A planetary boundary on freshwater use is misleading. *Hydrol. Earth Syst. Sci.* **21**, 3455–3461 (2017).
46. Bunsen, J., Berger, M. & Finkbeiner, M. Planetary boundaries for water – A review. *Ecol. Indic.* **121**, 107022 (2021).
47. Veldkamp, T. I. E. *et al.* Water scarcity hotspots travel downstream due to human interventions in the 20th and 21st century. *Nat. Commun.* **8**, 15697 (2017).
48. Rockström, J. *et al.* Planetary Boundaries: Exploring the Safe Operating Space for Humanity. *Ecol. Soc.* **14**, (2009).
49. Gerten, D. *et al.* Towards a revised planetary boundary for consumptive freshwater use: role of environmental flow requirements. *Curr. Opin. Environ. Sustain.* **5**, 551–558 (2013).
50. Huang, S. *et al.* Evaluation of an ensemble of regional hydrological models in 12 large-scale river basins worldwide. *Clim. Change* **141**, 381–397 (2017).
51. Veldkamp, T. I. E. *et al.* Human impact parameterizations in global hydrological models improve estimates of monthly discharges and hydrological extremes: a multi-model validation study. *Environ. Res. Lett.* **13**, 055008 (2018).
52. Zaherpour, J. *et al.* Worldwide evaluation of mean and extreme runoff from six global-scale hydrological models that account for human impacts. *Environ. Res. Lett.* **13**, 065015 (2018).

53. Zaherpour, J. *et al.* Exploring the value of machine learning for weighted multi-model combination of an ensemble of global hydrological models. *Environ. Model. Softw.* **114**, 112–128 (2019).

54. Zemp, D. C. *et al.* Self-amplified Amazon forest loss due to vegetation-atmosphere feedbacks. *Nat. Commun.* **8**, 14681 (2017).

55. Chrysafi, A. *et al.* Quantifying Earth system interactions for sustainable food production via expert elicitation. *Nat. Sustain.* **5**, 830–842 (2022).

56. Stevenson, S. *et al.* Twenty-first century hydroclimate: A continually changing baseline, with more frequent extremes. *Proc. Natl. Acad. Sci.* **119**, e2108124119 (2022).

57. Boulton, C. A., Lenton, T. M. & Boers, N. Pronounced loss of Amazon rainforest resilience since the early 2000s. *Nat. Clim. Change* **12**, 271–278 (2022).

58. Frieler, K. *et al.* Assessing the impacts of 1.5 °C global warming – simulation protocol of the Inter-Sectoral Impact Model Intercomparison Project (ISIMIP2b). *Geosci. Model Dev.* **10**, 4321–4345 (2017).

59. Telteu, C.-E. *et al.* Understanding each other's models: an introduction and a standard representation of 16 global water models to support intercomparison, improvement, and communication. *Geosci. Model Dev.* **14**, 3843–3878 (2021).

60. Taylor, K. E., Stouffer, R. J. & Meehl, G. A. An Overview of CMIP5 and the Experiment Design. *Bull. Am. Meteorol. Soc.* **93**, 485–498 (2012).

61. Lawrence, D. M. *et al.* The Community Land Model Version 5: Description of New Features, Benchmarking, and Impact of Forcing Uncertainty. *J. Adv. Model. Earth Syst.* **11**, 4245–4287 (2019).

62. Schaphoff, S. *et al.* LPJmL4 – a dynamic global vegetation model with managed land – Part 1: Model description. *Geosci. Model Dev.* **11**, 1343–1375 (2018).

63. Stacke, T. & Hagemann, S. Development and evaluation of a global dynamical wetlands extent scheme. *Hydrol. Earth Syst. Sci.* **16**, 2915–2933 (2012).

64. Sutanudjaja, E. H. *et al.* PCR-GLOBWB 2: a 5 arcmin global hydrological and water resources model. *Geosci. Model Dev.* **11**, 2429–2453 (2018).

65. Hanasaki, N. *et al.* An integrated model for the assessment of global water resources – Part 1: Model description and input meteorological forcing. *Hydrol. Earth Syst. Sci.* **12**, 1007–1025 (2008).

66. Takata, K., Emori, S. & Watanabe, T. Development of the minimal advanced treatments of surface interaction and runoff. *Glob. Planet. Change* **38**, 209–222 (2003).

67. Müller Schmied, H. *et al.* Variations of global and continental water balance components as impacted by climate forcing uncertainty and human water use. *Hydrol. Earth Syst. Sci.* **20**, 2877–2898 (2016).

68. Dunne, J. P. *et al.* GFDL's ESM2 Global Coupled Climate–Carbon Earth System Models. Part I: Physical Formulation and Baseline Simulation Characteristics. *J. Clim.* **25**, 6646–6665 (2012).

69. Collins, W. J. *et al.* Development and evaluation of an Earth-System model – HadGEM2. *Geosci. Model Dev.* **4**, 1051–1075 (2011).

70. Dufresne, J.-L. *et al.* Climate change projections using the IPSL-CM5 Earth System Model: from CMIP3 to CMIP5. *Clim. Dyn.* **40**, 2123–2165 (2013).

71. Watanabe, M. *et al.* Improved Climate Simulation by MIROC5: Mean States, Variability, and Climate Sensitivity. *J. Clim.* **23**, 6312–6335 (2010).

72. Chen, J. & Gupta, A. K. *Parametric statistical change point analysis: With applications to genetics, medicine, and finance*. (Birkhauser, Boston, USA, 2014).

73. Killick, R. & Eckley, I. A. changepoint: An R Package for Changepoint Analysis. *J. Stat. Softw.* **58**, 1–19 (2014).

74. Chambers, J., Hastie, T. & Pregibon, D. Statistical Models in S. in *Compstat* (eds. Momirović, K. & Mildner, V.) 317–321 (Physica-Verlag, Heidelberg, Germany, 1990).

75. Boé, J., Terray, L., Habets, F. & Martin, E. Statistical and dynamical downscaling of the Seine basin climate for hydro-meteorological studies. *Int. J. Climatol.* **27**, 1643–1655 (2007).

76. Gudmundsson, L. *et al.* Comparing Large-Scale Hydrological Model Simulations to Observed Runoff Percentiles in Europe. *J. Hydrometeorol.* **13**, 604–620 (2012).

77. Klein Goldewijk, K., Beusen, A., Doelman, J. & Stehfest, E. Anthropogenic land use estimates for the Holocene – HYDE 3.2. *Earth Syst. Sci. Data* **9**, 927–953 (2017).

78. Gädeke, A. *et al.* Performance evaluation of global hydrological models in six large Pan-Arctic watersheds. *Clim. Change* **163**, 1329–1351 (2020).

79. Food and Agriculture Organization of the United Nations (FAO). *Food and agriculture data statistics (FAOSTAT)* (FAO, 2022).

80. Wada, Y. & Bierkens, M. F. P. Sustainability of global water use: past reconstruction and future projections. *Environ. Res. Lett.* **9**, 104003 (2014).

81. Zarfl, C., Lumsdon, A. E., Berlekamp, J., Tydecks, L. & Tockner, K. A global boom in hydropower dam construction. *Aquat. Sci.* **77**, 161–170 (2015).

82. Keenan, R. J. *et al.* Dynamics of global forest area: Results from the FAO Global Forest Resources Assessment 2015. *For. Ecol. Manag.* **352**, 9–20 (2015).

83. Frieler, K. *et al.* Scenario set-up and forcing data for impact model evaluation and impact attribution within the third round of the Inter-Sectoral Model Intercomparison Project (ISIMIP3a). Preprint at doi:10.5194/egusphere-2023-281.

Acknowledgements

We would like to acknowledge Will Steffen – who sadly passed away during the writing of this paper – and Katherine Richardson for the discussions related to planetary boundaries, and the ISIMIP team and all participating modelling teams for making the outputs available.

Funding

European Research Council under the European Union's Horizon 2020 research and innovation programme (grant no. 819202) (MP, MK)

Erling-Persson Family Foundation (MP)

Aalto University School of Engineering Doctoral Programme (VV)

European Research Council through the "Earth Resilience in the Anthropocene" project (grant no. ERC-2016-ADG 743080) (LWE, IF, AT, JR)

IKEA Foundation (LWE)

Formas - A Swedish Research Council for Sustainable Development (grant no. 2022-02089) (LWE)

Academy of Finland-funded project WATVUL (grant no. 317320) (MK)

The Netherlands Organization for Scientific Research (NWO), project number 016.Veni.181.015 (RvdE)

Competing interests

Authors declare that they have no competing interests.

Additional information

Supplementary material includes Supplementary text and Table S1. Extended Data Figures 1–8 are attached to this document.

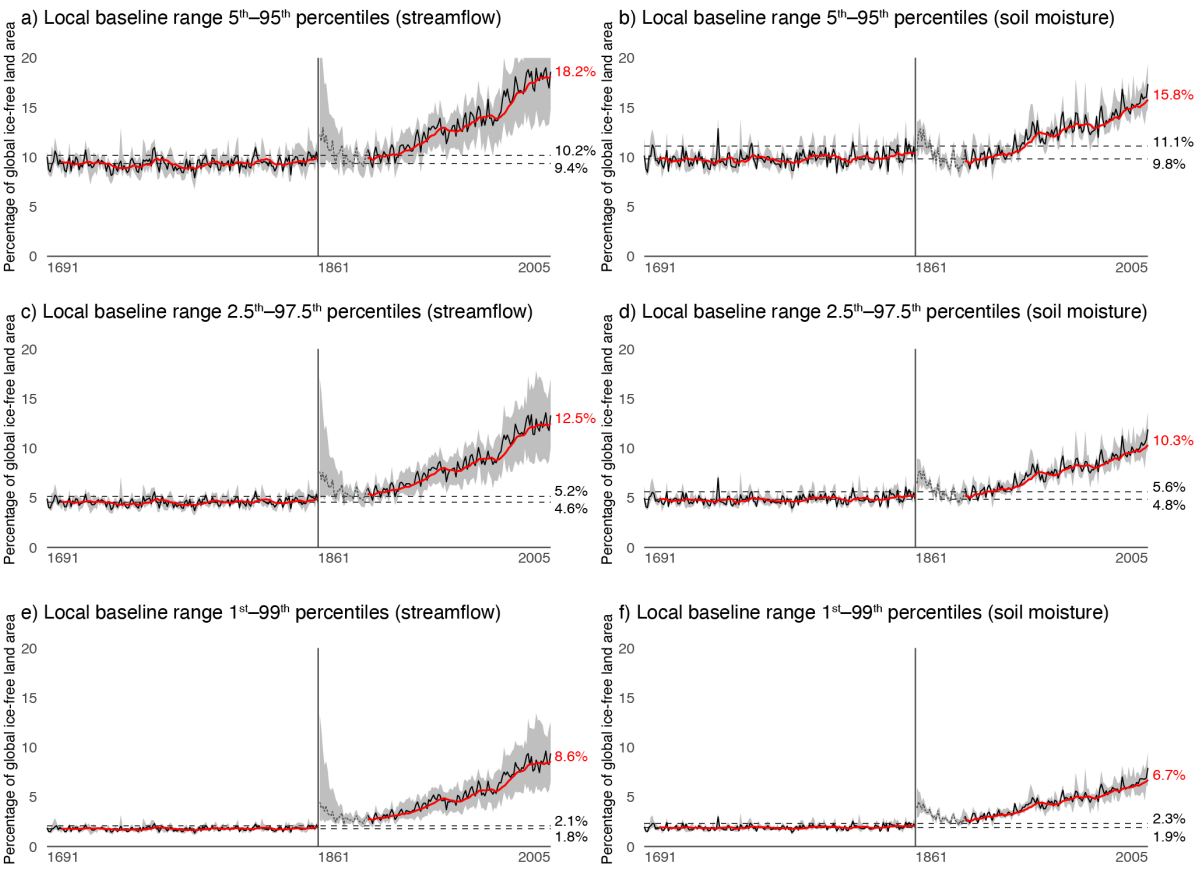

Extended Data Fig. 1. Percentage of global ice-free land area with local streamflow (a, c, e) and soil moisture (b, d, f) deviations, using variable bounds of the local baseline range. Panels show the percentage of land area with local deviations (Fig. 1c) when the local baseline range (Fig. 1a) is defined as the 5th–95th (a–b), 2.5th –97.5th (c–d) or 1st–99th (e–f) percentile range. Panels a–b correspond to Fig. 2 and Extended Data Fig. 6a, d. Shown is the annual percentage, which is computed as an average of monthly percentages. The ensemble median (solid black line) and interquartile range (grey shading) are computed from n = 23 (streamflow) and n = 15 (soil moisture) ensemble members. The horizontal dashed lines drawn in each panel denote the median and the upper end of pre-industrial variability (Fig. 1d), and the current (mean of 1996–2005) percentage of land area with local deviations is annotated at the end of the red 10-year moving (trailing) mean line. Values prior to 1691 are excluded and the ensemble median line for 1861–1890 is shaded and dashed due to traces of model spinups being common during these years (Extended Data Fig. 2–3).

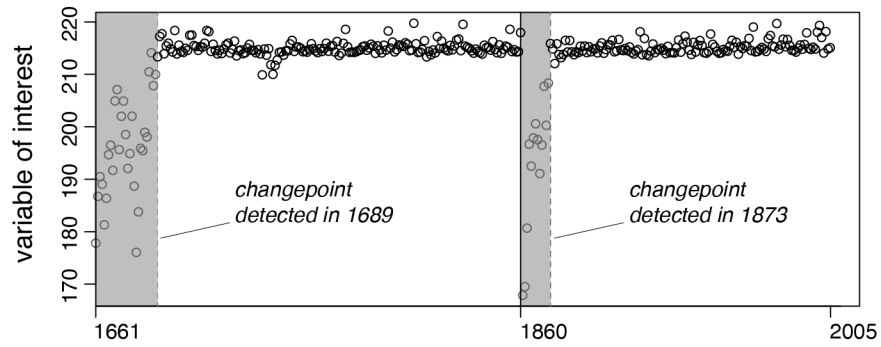

Extended Data Fig. 2. An example case of detecting the most likely changepoints in mean and variance. Values shown in the plot describe soil moisture in one grid cell, for one month, and for one ensemble member. As the changepoints are detected between 10 and 30 years from the initiation of each simulation period, they are considered as traces of model spinup (Methods). Hence, values shaded in grey are excluded from distribution shift correction (Extended Data Fig. 3) and from setting the local baseline range (Fig. 1a).

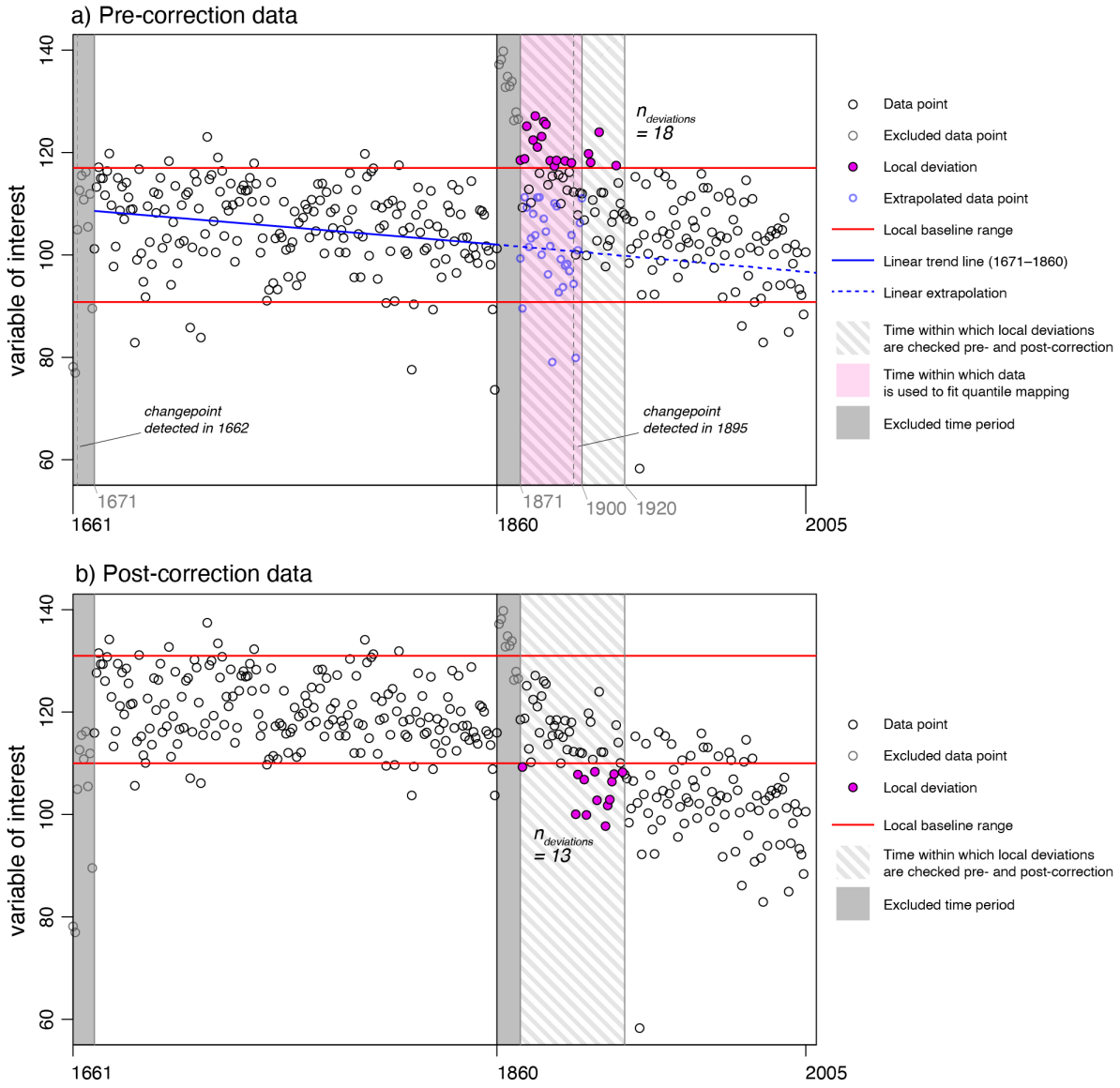

Extended Data Fig. 3. Correcting shifts in cell-wise value distribution around the year 1860 transition point between pre-industrial and industrial ISIMIP 2b simulations. Values shown in the plot describe soil moisture in one grid cell, for one month, and for one ensemble member. Black circles show data prior to correction (a) and after the correction (b). Linear trend (blue line) is estimated and extrapolated excluding the ten first pre-industrial values (i.e. years 1671–1860). For the period highlighted with pink shading, quantile mapping is fitted between industrial simulation values and values following the linear extrapolation line with added random normal noise (blue circles). Once quantile mapping is applied for pre-industrial data points, resulting in panel b, the number of local deviations (purple filled circles) outside the local baseline range (red lines) is compared pre- and post-correction for a period of 50 years (striped shading). Should the number of local deviations decrease, as is the case here, the corrected values (panel b) are accepted, otherwise the uncorrected values (panel a) would be retained. See Methods for details.

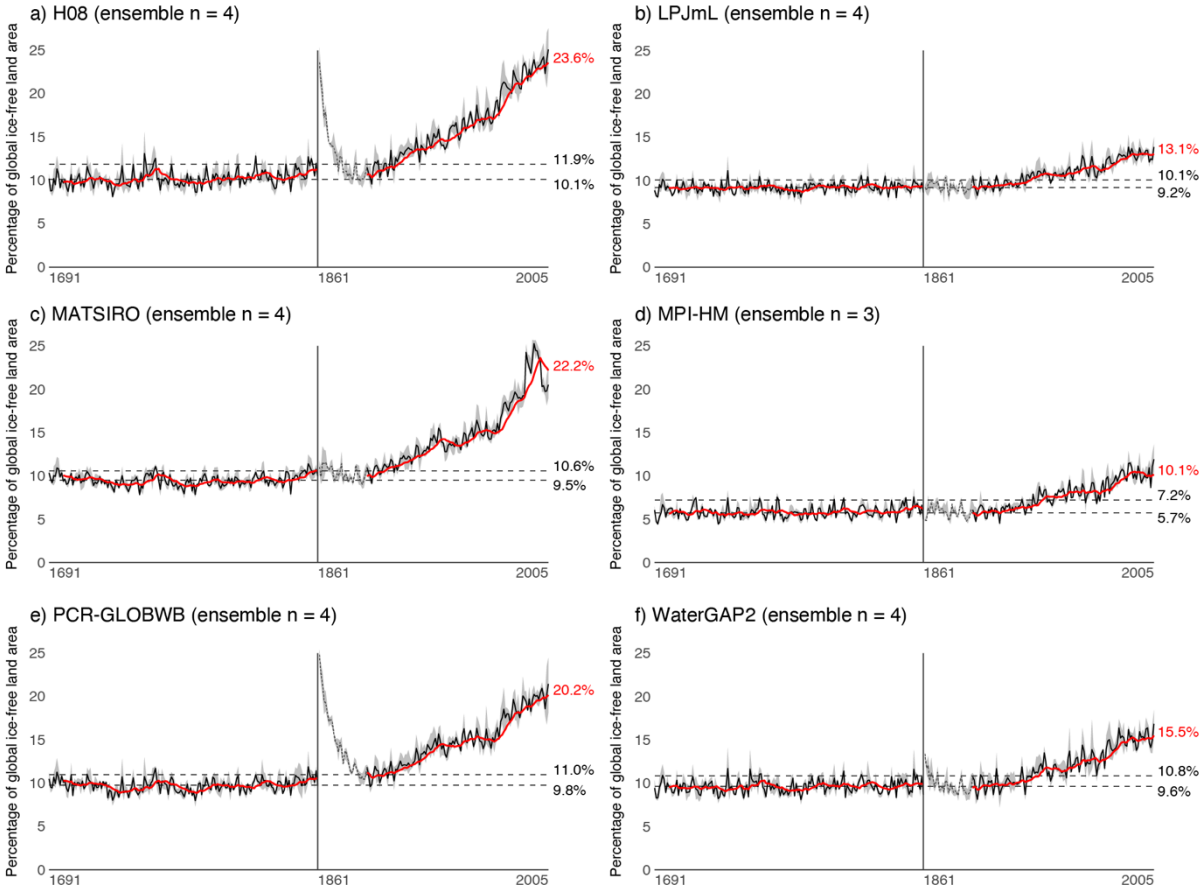

Extended Data Fig. 4. Percentage of global ice-free land area with local streamflow deviations, separately for global hydrological models (GHMs) included in this study. Panels describe the percentage of land area with local deviations (Fig. 1c) for H08 (a), LPJmL (b), MATSIRO (c), MPI-HM (d), PCR-GLOBWB (e), and WaterGAP2 (f). Shown is the annual percentage, which is computed as an average of monthly percentages. The horizontal dashed lines drawn in each panel denote the median and the upper end of pre-industrial variability (Fig. 1d), and the current (mean of 1996–2005) percentage of land area with local deviations is annotated at the end of the red 10-year moving (trailing) mean line. The ensemble median and interquartile range (grey shading) are computed from n = 3–4 members (number of GCMs), as data forced with HadGEM2 were not available MPI-HM. The ensemble median line for 1861–1890 is shaded and dashed due to traces of model spinups being common during these years (especially a, e).

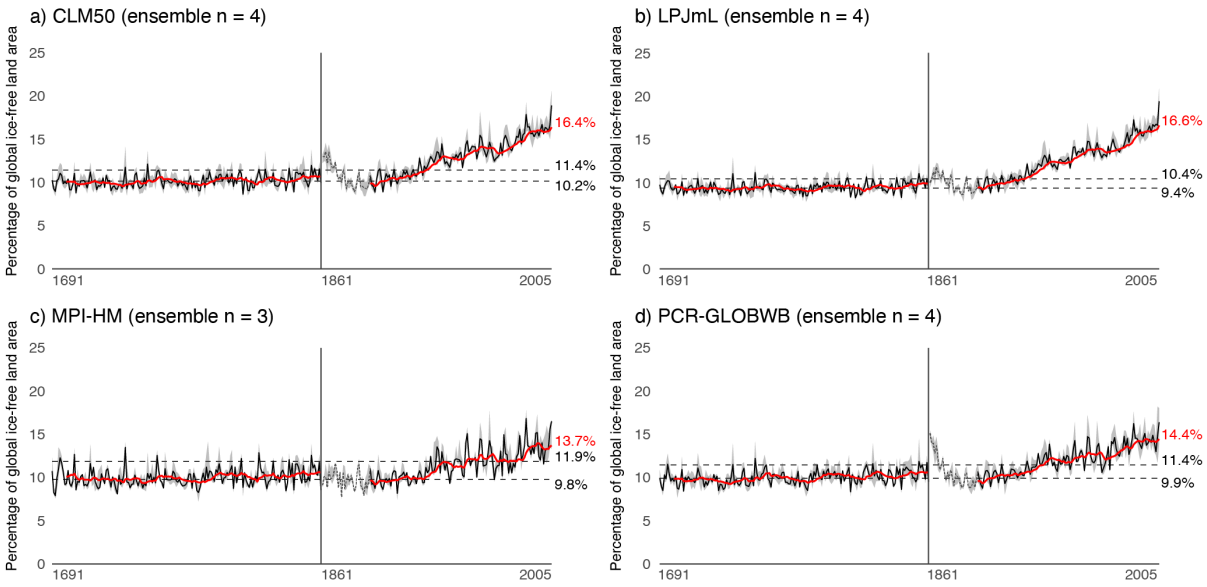

Extended Data Fig. 5. Percentage of global ice-free land area with local soil moisture deviations, separately for global hydrological models (GHMs) included in this study. Panels describe the percentage of land area with local deviations (Fig. 1c) for CLM50 (a), LPJmL (b), MPI-HM (c), and PCR-GLOBWB (d). Shown is the annual percentage, which is computed as an average of monthly percentages. The horizontal dashed lines drawn in each panel denote the median and the upper end of pre-industrial variability (Fig. 1d), and the current (mean of 1996–2005) percentage of land area with local deviations is annotated at the end of the red 10-year moving (trailing) mean line. The ensemble median and interquartile range (grey shading) are computed from n = 3–4 members (number of GCMs), as data forced with HadGEM2 were not available for MPI-HM. The ensemble median line for 1861–1890 is shaded and dashed due to traces of model spinups being common during these years (especially a, d).

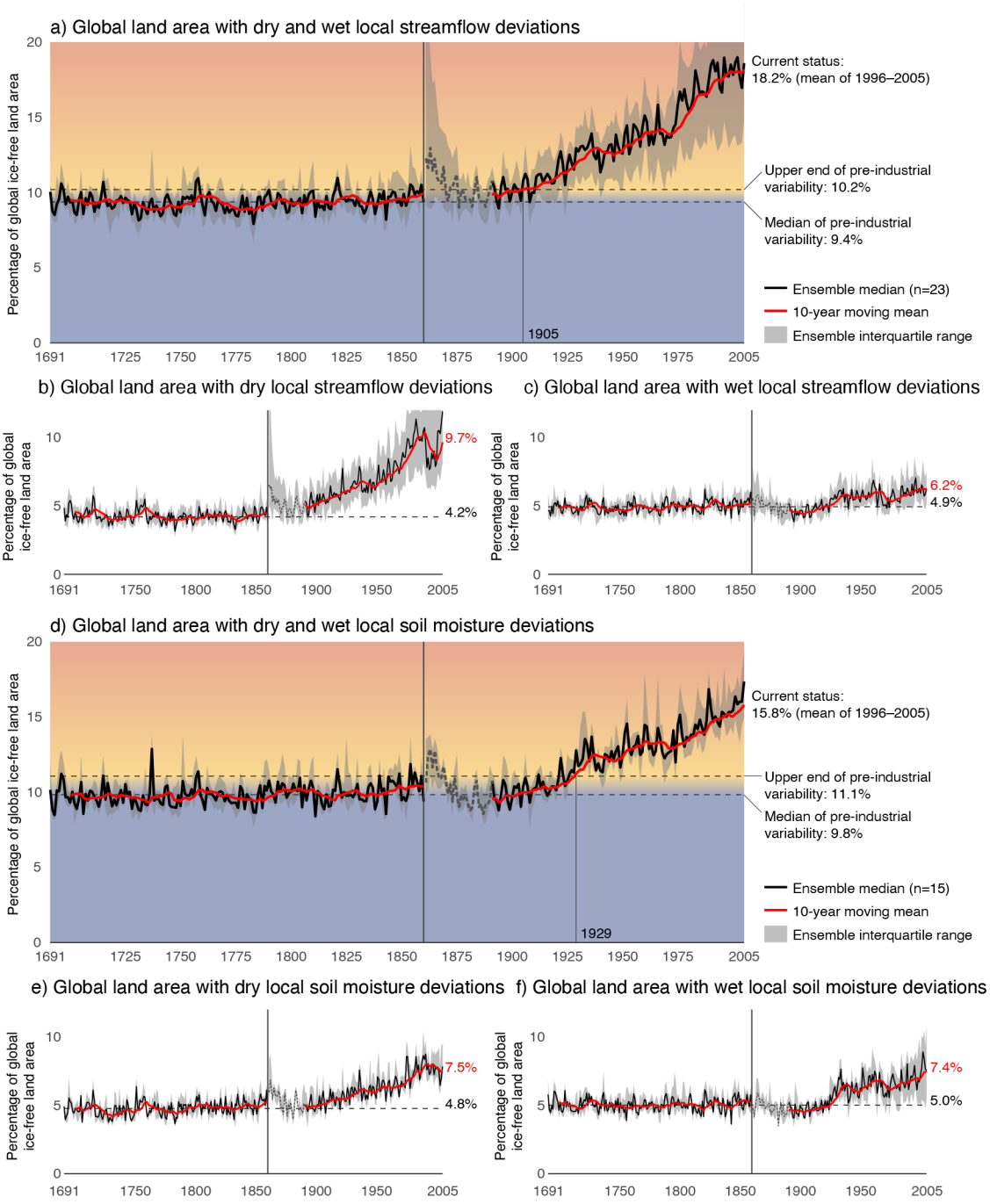

Extended Data Fig. 6. Percentage of global ice-free land area with local streamflow (a–c) and soil moisture (d–e) deviations, dry and wet local deviations summed (a, d), and for dry (b, e) and wet (c, f) local deviations separately. Shown is the annual percentage, which is computed as an average of monthly percentages. The annotated years mark the 10-year moving (trailing) mean transgressing the upper end of pre-industrial variability (95th percentile of the pre-industrial percentage of land area with local deviations; Fig. 1d). The ensemble median and interquartile range are computed from n = 23 (streamflow) and n = 15 (soil moisture) ensemble members. Values prior to 1691 are excluded and the ensemble median line for 1861–1890 is shaded and dashed due to traces of model spinups being common during these years (Extended Data Fig. 2–3).

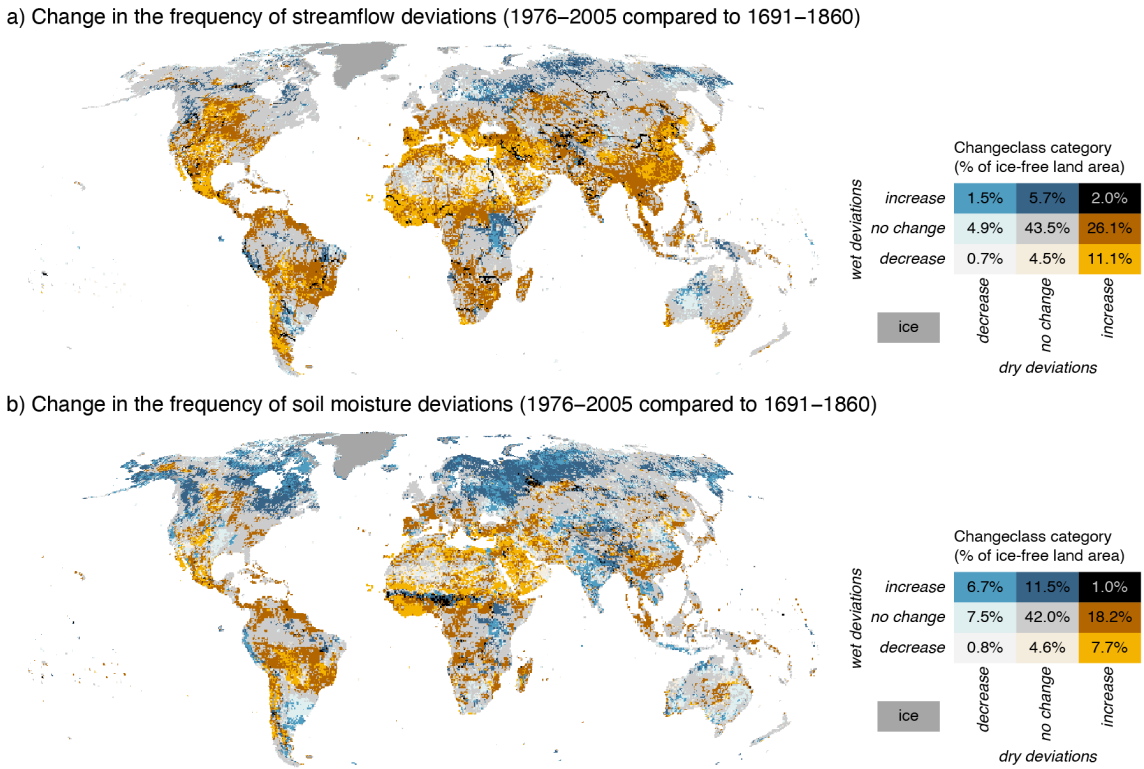

Extended Data Fig. 7. Statistically significant changes in dry and wet local deviation frequency for streamflow (a) and for soil moisture (b). Changes in the frequency of local deviations are computed by comparing the ensemble median frequency of local deviations during 1976–2005 against 1691–1860, and significance of change is tested at a 95% confidence level (p = 0.05) with R package *stats* function *prop.test*[29]. The changes are classified according to the direction of change (decreasing or increasing frequency of deviations) but with no regards to magnitude. Percentage shares of ice-free land area covered by each class are represented in the bivariate legend.

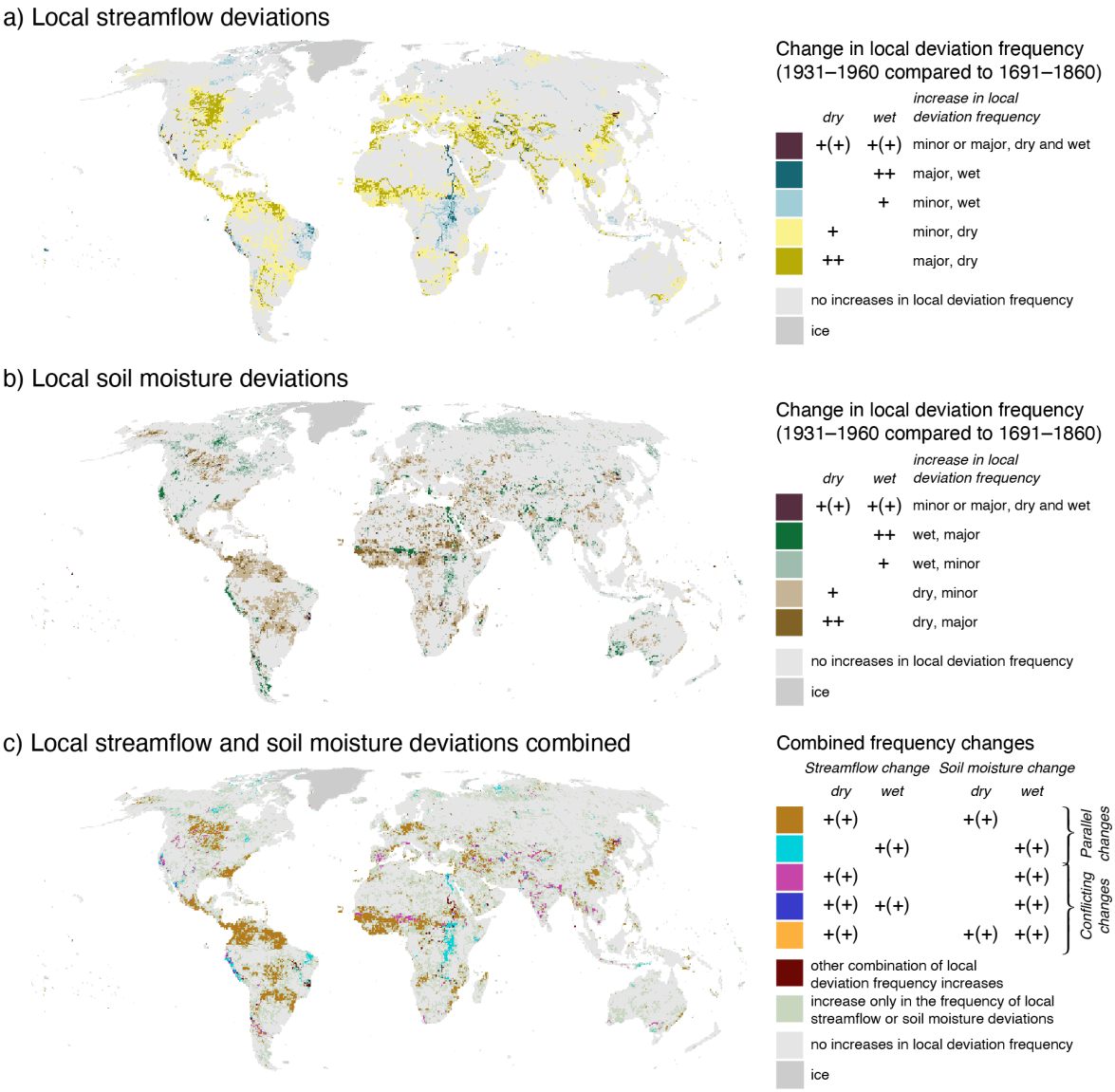

Extended Data Fig. 8. Statistically significant increases in dry and wet local deviation frequency for streamflow (a), for soil moisture (b), and combined for streamflow and soil moisture (c). Changes in the frequency of local deviations are computed by comparing the ensemble median frequency of local deviations during 1931–1960 against 1691–1860, and significance of change is tested at a 95% confidence level (p = 0.05) with R package *stats* function *prop.test*[29]. Colours denoted with + indicate statistically significant increases with magnitude less than 5 pp (minor), whereas colours denoted with ++ indicate statistically significant increases with magnitude greater than 5 pp (major). Colours denoted with +(+) pool together any statistically significant increase (minor or major).

Supplementary material for

Global water cycle shifts far beyond pre-industrial conditions – planetary boundary for freshwater change transgressed

Miina Porkka†, Vili Virkki†, Lan Wang-Erlandsson, Dieter Gerten, Tom Gleeson, Chinchu Mohan, Ingo Fetzer, Fernando Jaramillo, Arie Staal, Sofie te Wierik, Arne Tobian, Ruud van der Ent, Petra Döll, Martina Flörke, Simon N. Gosling, Naota Hanasaki, Yusuke Satoh, Hannes Müller Schmied, Niko Wanders, Johan Rockström, Matti Kummu

†These authors contributed equally to this work
Correspondence to: miina.porkka@aalto.fi, vili.virkki@aalto.fi

This Supplementary material includes:

Supplementary text

Table S1

References

Supplementary text

Freshwater supports terrestrial and aquatic ecosystems, mediates flows of material and energy, and regulates the Earth's climate. It is therefore tightly coupled with the core planetary boundaries (PBs) of climate change and biosphere integrity, as well as the land-system change and biogeochemical flows boundaries[1,2]. As the novel entities and biogeochemical flows PBs can be considered to (implicitly) cover quality aspects of freshwater, the freshwater PB focuses on the quantity of water. While justifiably included in the planetary boundaries framework, the current freshwater planetary boundary definition has been criticised for not reflecting all critical Earth system functions of water, not capturing the impact of all major anthropogenic drivers and failing to recognise the interplay between local and global drivers and impacts[3–6].

Initially, the freshwater use PB was defined by annual global *blue water* (surface and groundwater) consumption as a proxy control variable that reflects precipitation partitioning into blue and *green water* (terrestrial evaporation and soil moisture) flows and stocks, and integrates the anthropogenic drivers impacting them[7]. The original assessment[7] estimated human modifications of freshwater to be within safe boundaries, but later estimates with more nuanced quantification of water availabilities[8] and water consumption – by explicitly including also consumptive use of green water[5] – suggested that the PB is either being rapidly approached or has already been transgressed. Nevertheless, an update of the PB framework[9] still concluded that the globally aggregated status of the freshwater use PB is safe. However, transgressions were recognised at the basin scale, where safe boundaries were set based on minimum acceptable levels of river flows to maintain an adequate state of aquatic ecosystems[9]. Recently – to respond to the ambiguity and criticisms around the freshwater PB – studies have proposed sub-dividing the freshwater PB into blue and green water components and adopting a bottom-up, area-based approach[3,10,11]. The provisional analysis of Wang-Erlandsson et al.[11] proposed that the freshwater PB should describe *change* rather than *use*, and found a likely transgression of the green water component.

We follow Wang-Erlandsson et al.[11] in proposing to replace the original *freshwater use PB* with two control variables for *freshwater change*, measuring the global area with streamflow (blue water) or root-zone soil moisture (hereinafter referred to as soil moisture; green water) deviations from the range of local pre-industrial variability. Our approach is based on Wang-Erlandsson et al.[11] who suggested complementing the freshwater PB with a provisional green water component, while we unify the blue and green water components under one assessment. Widespread deviations from the relatively undisturbed pre-industrial state can be considered to pose elevated risks to the Earth system functions of freshwater. For example, terrestrial and freshwater ecosystems have adapted to specific quantities and timing of water flows[12–14], and wetness of landscapes regulates climate from micro- to regional and global scales, such that changes in (timing of) wetness in one location can impact rainfall and consequently streamflow and soil moisture both locally and remotely[15].

By extending the freshwater PB to cover both blue and green water components, our approach allows 1) representing the extent and impacts of freshwater change not only with respect to aquatic ecosystems but also across terrestrial biomes and ecosystems; and 2) allowing consistent comparison of the blue and green water components. Neither of these can be represented by the previous freshwater PB (water use & environmental flows). Another key

advantage of our approach is that calculating the blue and green water metrics using coherent methodology allows us to assess their coevolution. This is very important for a comprehensive analysis of freshwater change, as comparable metrics allow for inferring the nature of change (e.g. how other elements of the water cycle may have changed or what might be driving the change). Furthermore, the methodology applied here is transferable to additional variables in future studies. The previous methods of assessing the freshwater PB lack these factors, which is why we use a more general approach.

Our green water control variable aligns with Wang-Erlandsson et al.[11] who suggested, after an extensive literature review, that root-zone soil moisture is the most suitable control variable for representing the Earth system functions of green water. For blue water, we select streamflow as our control variable because streamflow alterations are either directly or indirectly connected to most major anthropogenic modifications and Earth system functions of blue water. These include e.g. water withdrawals, flow regulation, and groundwater depletion, as well as key Earth system functions, such as aquatic habitat provision and storage and transport of carbon and nutrients[10]. As streamflow is also impacted by anthropocentric climate change[16], it is a suitable control variable to represent the Earth system functions of blue water in aggregate. In addition to an adequate representation of the human drivers and Earth system impacts of freshwater change, the selected control variables are routinely simulated by global hydrological models and can therefore be updated on an annual basis. The variables can, in principle, also be observed directly, e.g. by in situ measurements or remote sensing[17,18], though spatial and temporal coverage of observational data is currently not sufficient for a comprehensive global analysis such as the one presented here.

The planetary boundaries framework[7,9] considers the Holocene geological epoch as the desired reference conditions prior to extensive anthropogenic forcing. However, as major spatial shifts of the water cycle have occurred since the Holocene[19,20], strictly grid cell scale comparisons – as those done here – are not meaningful using a Holocene baseline. Hence, we selected the pre-industrial period as our comparison baseline, also because of the wide availability of consistent and comparable ISIMIP 2b data[21]. By grounding our analysis in the pre-industrial period, we were able to establish our reference conditions before substantial anthropogenic modifications of the water cycle, including e.g. large dams[22], large scale irrigation systems[23], the rapid increase of intensive land uses[24], and anthropocentric climate change[16]. Therefore, we assumed that the pre-industrial period represents Holocene-like conditions – and that widespread deviations from that 'pristine' state are problematic.

Based on our analysis, the freshwater change PB has been transgressed since the early 20th century, for both blue and green water components. Currently, 18.2% and 15.8% of global ice-free land area experience local deviations that occurred only on approximately 9–10% of land area during the pre-industrial time. Given that variability in this percentage during the pre-industrial period is small (~ 3 pp), these changes are substantial and clearly indicate a shift in the global water cycle. This means that extreme conditions – both wet and dry – are occurring more often than before the onset of major anthropogenic drivers of change. The water cycle has thus shifted to a state in which it has not been in during the development of contemporary human societies. Therefore, humanity's risks related to the Earth system functions of freshwater may be elevated.

Our new freshwater change PB definition is associated with two main kinds of uncertainties: 1) the ability of our control variables to represent Earth system change and 2) placement of the boundary value of freshwater change and assessing what its transgression means for the Earth system. Streamflow and soil moisture do not represent all freshwater changes – such as water quality aspects – and omit explicit consideration of other freshwater flows and stocks, such as groundwater and land ice. From the perspective of the PB framework, however, these choices can be justified, as water quality is (implicitly) considered in the PBs of Biogeochemical flows and Novel entities[7,9], and because such an overarching framework requires expressing very complex Earth system processes in relatively simple terms. Nonetheless, a more comprehensive assessment of humanity's overall impact on the freshwater cycle would require careful consideration of the many complex relationships between drivers, hydrological responses and their Earth system impacts that weren't explicitly considered in this analysis.

Major uncertainties remain also regarding the planetary boundary value of freshwater change – that is, which level of freshwater change would trigger state changes in the Earth system or increase gradual risks at an unacceptable rate. Although impacts of freshwater change on the Earth system functions of freshwater have been studied extensively at local to regional scales[10], regional to planetary scale impact assessments are still lacking. Furthermore, the PBs' control variables – including freshwater – interact strongly with each other[1,2], which should be considered when setting a PB for freshwater change. These factors complicate the boundary setting, as ideally, PBs should be set based on control variable–response variable relationships to minimise the risk of abrupt or irreversible state shifts. In the absence of such assessments, we chose to set the boundary at the upper end of the pre-industrial, Holocene-like variability range, as it represents conditions that were present before major anthropogenic alterations of the freshwater cycle. It is possible, however, that the intrinsic resilience of the Earth system will maintain a Holocene-like state even if the pre-industrial range of variability is exceeded – as it has already been for a long time. However, as the extent of a 'safe' exceedance cannot be robustly defined without quantifications of Earth system-wide responses of freshwater change, we applied the precautionary principle of the PB framework[7,25], and set the boundary at the lower end of scientific uncertainty. We consider this to be at the upper end (95th percentile) of pre-industrial variability range, which can be regarded as highly precautionary – although an even stricter boundary placement could also be justified, due to signs of weakened Earth system resilience[11] and the complex interactions between freshwater and other PBs[1,2].

simulation period	climate scenario	socio-economic conditions	ISIMIP output variable	GHM	GCMs
pre-industrial	picontrol	1860soc	rootmoist	CLM50	GFDL-ESM2M, HadGEM2-ES, IPSL-CM5A-LR, MIROC5
pre-industrial	picontrol	1860soc	rootmoist	LPJmL	GFDL-ESM2M, HadGEM2-ES, IPSL-CM5A-LR, MIROC5
pre-industrial	picontrol	1860soc	rootmoist	MPI-HM	GFDL-ESM2M, IPSL-CM5A-LR, MIROC5
pre-industrial	picontrol	1860soc	rootmoist	PCR-GLOBWB	GFDL-ESM2M, HadGEM2-ES, IPSL-CM5A-LR, MIROC5
pre-industrial	picontrol	1860soc	dis	H08	GFDL-ESM2M, HadGEM2-ES, IPSL-CM5A-LR, MIROC5
pre-industrial	picontrol	1860soc	dis	LPJmL	GFDL-ESM2M, HadGEM2-ES, IPSL-CM5A-LR, MIROC5
pre-industrial	picontrol	1860soc	dis	MATSIRO	GFDL-ESM2M, HadGEM2-ES, IPSL-CM5A-LR, MIROC5
pre-industrial	picontrol	1860soc	dis	MPI-HM	GFDL-ESM2M, IPSL-CM5A-LR, MIROC5
pre-industrial	picontrol	1860soc	dis	PCR-GLOBWB	GFDL-ESM2M, HadGEM2-ES, IPSL-CM5A-LR, MIROC5
pre-industrial	picontrol	1860soc	dis	WaterGAP2	GFDL-ESM2M, HadGEM2-ES, IPSL-CM5A-LR, MIROC5
historical	historical	histsoc	rootmoist	CLM50	GFDL-ESM2M, HadGEM2-ES, IPSL-CM5A-LR, MIROC5
historical	historical	histsoc	rootmoist	LPJmL	GFDL-ESM2M, HadGEM2-ES, IPSL-CM5A-LR, MIROC5
historical	historical	histsoc	rootmoist	MPI-HM	GFDL-ESM2M, IPSL-CM5A-LR, MIROC5
historical	historical	histsoc	rootmoist	PCR-GLOBWB	GFDL-ESM2M, HadGEM2-ES, IPSL-CM5A-LR, MIROC5
historical	historical	histsoc	dis	H08	GFDL-ESM2M, HadGEM2-ES, IPSL-CM5A-LR, MIROC5
historical	historical	histsoc	dis	LPJmL	GFDL-ESM2M, HadGEM2-ES, IPSL-CM5A-LR, MIROC5
historical	historical	histsoc	dis	MATSIRO	GFDL-ESM2M, HadGEM2-ES, IPSL-CM5A-LR, MIROC5
historical	historical	histsoc	dis	MPI-HM	GFDL-ESM2M, IPSL-CM5A-LR, MIROC5
historical	historical	histsoc	dis	PCR-GLOBWB	GFDL-ESM2M, HadGEM2-ES, IPSL-CM5A-LR, MIROC5
historical	historical	histsoc	dis	WaterGAP2	GFDL-ESM2M, HadGEM2-ES, IPSL-CM5A-LR, MIROC5

Table S1. Data sets used in this study, adopting ISIMIP 2b nomenclature[21]. The *pre-industrial* simulation period represents 200 years of pre-industrial conditions, nominally covering years 1661–1860, and the *historical* simulation period covers years 1861–2005. The climate scenario *picontrol* uses pre-industrial climate and 286 ppm CO2 concentration, while the *historical* climate scenario uses historical climate and CO2 concentration. Socio-economic conditions for the scenario *1860soc* are fixed at the pre-industrial level, while the *histsoc* scenario uses varying historical land use and socio-economic conditions. The ISIMIP output variables *rootmoist* and *dis* refer to root-zone soil moisture (soil moisture) and discharge (streamflow), respectively.

References

1. Chrysafi, A. *et al.* Quantifying Earth system interactions for sustainable food production via expert elicitation. *Nat. Sustain.* **5**, 830–842 (2022).
2. Lade, S. J. *et al.* Human impacts on planetary boundaries amplified by Earth system interactions. *Nat. Sustain.* **3**, 119–128 (2020).
3. Gleeson, T. *et al.* The Water Planetary Boundary: Interrogation and Revision. *One Earth* **2**, 223–234 (2020).
4. Heistermann, M. HESS Opinions: A planetary boundary on freshwater use is misleading. *Hydrol. Earth Syst. Sci.* **21**, 3455–3461 (2017).
5. Jaramillo, F. & Destouni, G. Local flow regulation and irrigation raise global human water consumption and footprint. *Science* **350**, 1248–1251 (2015).
6. Molden, D. Planetary boundaries: The devil is in the detail. *Nat. Clim. Change* **1**, 116–117 (2009).
7. Rockström, J. *et al.* Planetary Boundaries: Exploring the Safe Operating Space for Humanity. *Ecol. Soc.* **14**, (2009).
8. Gerten, D. *et al.* Towards a revised planetary boundary for consumptive freshwater use: role of environmental flow requirements. *Curr. Opin. Environ. Sustain.* **5**, 551–558 (2013).
9. Steffen, W. *et al.* Planetary boundaries: Guiding human development on a changing planet. *Science* **347**, 1259855 (2015).
10. Gleeson, T. *et al.* Illuminating water cycle modifications and Earth system resilience in the Anthropocene. *Water Resour. Res.* **56**, e2019WR024957 (2020).
11. Wang-Erlandsson, L. *et al.* A planetary boundary for green water. *Nat. Rev. Earth Environ.* **3**, 380–392 (2022).
12. Berdugo, M. *et al.* Global ecosystem thresholds driven by aridity. *Science* **367**, 787–790 (2020).
13. Meir, P. *et al.* Threshold Responses to Soil Moisture Deficit by Trees and Soil in Tropical Rain Forests: Insights from Field Experiments. *BioScience* **65**, 882–892 (2015).
14. Richter, B., Baumgartner, J., Wigington, R. & Braun, D. How much water does a river need? *Freshw. Biol.* **37**, 231–249 (1997).
15. Wang-Erlandsson, L. *et al.* Remote land use impacts on river flows through atmospheric teleconnections. *Hydrol. Earth Syst. Sci.* **22**, 4311–4328 (2018).
16. Gudmundsson, L. *et al.* Globally observed trends in mean and extreme river flow attributed to climate change. *Science* **371**, 1159–1162 (2021).
17. Birkinshaw, S. J. *et al.* Daily discharge estimation at ungauged river sites using remote sensing. *Hydrol. Process.* **28**, 1043–1054 (2014).
18. Peng, J., Loew, A., Merlin, O. & Verhoest, N. E. C. A review of spatial downscaling of satellite remotely sensed soil moisture. *Rev. Geophys.* **55**, 341–366 (2017).

19. Dallmeyer, A., Claussen, M., Lorenz, S. J. & Shanahan, T. The end of the African humid period as seen by a transient comprehensive Earth system model simulation of the last 8000 years. *Clim. Past* **16**, 117–140 (2020).

20. Dallmeyer, A. *et al.* Holocene vegetation transitions and their climatic drivers in MPI-ESM1.2. *Clim. Past* **17**, 2481–2513 (2021).

21. Frieler, K. *et al.* Assessing the impacts of 1.5 °C global warming – simulation protocol of the Inter-Sectoral Impact Model Intercomparison Project (ISIMIP2b). *Geosci. Model Dev.* **10**, 4321–4345 (2017).

22. Lehner, B. *et al.* High-resolution mapping of the world's reservoirs and dams for sustainable river-flow management. *Front. Ecol. Environ.* **9**, 494–502 (2011).

23. Siebert, S. *et al.* A global data set of the extent of irrigated land from 1900 to 2005. *Hydrol. Earth Syst. Sci.* **19**, 1521–1545 (2015).

24. Ellis, E. C. *et al.* People have shaped most of terrestrial nature for at least 12,000 years. *Proc. Natl. Acad. Sci.* **118**, (2021).

25. Kriebel, D. *et al.* The precautionary principle in environmental science. *Environ. Health Perspect.* **109**, 871–876 (2001).